A COUPLED MODELING SYSTEM TO PREDICT MORPHOLOGY CHANGES AND A COMPARISON OF PRESSURE GRADIENT FORCES TO SHEAR STRESSES IN THE NEARSHORE

By

WILLIAM L. REILLY

A THESIS PRESENTED TO THE GRADUATE SCHOOL
OF THE UNIVERSITY OF FLORIDA IN PARTIAL FULFILLMENT
OF THE REQUIREMENTS FOR THE DEGREE OF
MASTER OF SCIENCE

UNIVERSITY OF FLORIDA

2005

This work is dedicated to my mother, father, and sister.

ACKNOWLEDGMENTS

I wish to thank my friends and family for their continued support and encouragement. I would not be where I am today if it was not for the guidance, direction, and advice of my wonderful family. It is my close friends and everyone that have meant something to me along the way that makes me who I am today.

Dr. Donald Slinn, my graduate advisor, must be acknowledged for his continued support, not only academically but also in his efforts of helping me with my future endeavors. I also thank Dr. Robert Thieke and Dr. Ashish Mehta for taking the time to serve on my committee. I must also thank the other professors at the University of Florida in the Civil and Coastal Engineering Department for their dedication and effort of sharing their knowledge to the next generation of coastal engineers.

Lastly, I would like to acknowledge a few other people who have made this project possible. Appreciation is given to Bill Birkemeier for his help in my growth of an aspiring engineer as well as the Field Research Facility for providing the data for this project. Finally, I would like to thank Nathaniel Plant as well as the other members of the Naval Research Lab for their continued support on this project.

TABLE OF CONTENTS

LIST OF FIGURES

Abstract of Thesis Presented to the Graduate School
of the University of Florida in Partial Fulfillment of the
Requirements for the Degree of Master of Science

A COUPLED MODELING SYSTEM TO PREDICT MORPHOLOGY CHANGES AND A COMPARISON OF PRESSURE GRADIENT FORCES TO SHEAR STRESSES IN THE NEARSHORE

By

William L. Reilly

August 2005

Chair: Donald Slinn
Major Department: Civil and Coastal Engineering

Two separate, but related, topics are investigated in this study. The goal of the first half of the study is to simulate beach morphology on time scales of hours to days. Our approach is to develop finite difference solutions from a coupled modeling system consisting of nearshore wave, circulation, and sediment flux models. We initialize the model with bathymetry from a dense data set north of the pier at the Field Research Facility (FRF) in Duck, NC. The offshore wave height and direction are taken from the 8-meter bipod at the FRF and input to the wave-model, SWAN (Spectral WAve Nearshore). The resulting calculated wave induced force per unit surface area (gradient of the radiation stress) output from SWAN is used to drive the currents in our circulation model. Our hydrodynamic model is then integrated forward in time solving the 2-dimensional unsteady Navier Stokes Equations. The divergence of the time averaged sediment flux is calculated after one hour of simulation. The sediment flux model is

based on the energetics approach of Bagnold and includes approximations for both bed-load and suspended load.

The results of bathymetric change vary for different wave conditions. Typical results indicate that for wave heights on the order of one meter, shoreline advancement and sandbar evolution is observed on the order of tens of centimeters. While the magnitudes of the resulting bathymetric changes seem to be smaller than expected, the general shape and direction of transport appear to be reasonable.

The second half of this study takes a systematic look at the ratio of horizontal forces on the seabed from shear stresses compared to the forces exerted by the pressure gradients of passing waves. This study was completed to investigate the importance of these pressure gradients to sediment transport. We develop analytic solutions, for linear and weakly nonlinear waves, to predict the forces felt by individual sand grains by passing waves. A range of wave frequencies and amplitudes, water depths, and grain sizes are varied to calculate the two horizontal forces.

We demonstrate that the pressure gradient, for certain sediment sizes and wave regimes, can be sufficient to induce bed motion. A principal consequence of our findings is that near shore sediment transport parameterizations should not be based upon empirical relationships developed from steady open channel or even oscillatory flow experiments if they are not produced by surface gravity waves. This work will also help in the parameterization of sediment flux in the direction of wave advance due to asymmetric and skewed nonlinear wave shapes typical of shoaled and breaking waves.

CHAPTER 1
OVERVIEW

1.1 Preface

Accurate predictions of nearshore bathymetric change are challenging at all relevant scales. The difficulty lies in that the relevant scales span a very broad range. One could look at a very small scale process such as grain to grain interaction (*O* millimeters) or how a sandbar moves from a pre-storm position to a post-storm position (*O* meters) or even the scope of alongshore littoral cells (*O* kilometers). The largest spatial scales are of particular importance because they contain the majority of the spatial and temporal variability of nearshore bathymetric change [Lippmann and Holman, 1990; Plant et al., 1999]. In terms of temporal scales, similar breadth is encountered. One could look at very short time scales such as turbulent dissipation (*O* seconds) or tidal influence on sediment transport (*O* hours) or even chronic erosion (*O* years). To complicate things further, sediment suspension observed in the surf zone is also spatially and temporally intermittent on time periods of waves, storms, seasons or climate variability. Large changes in concentration occur over times shorter than a wave period [e.g., Downing et al., 1981] and at spatial scales shorter than a wavelength. The difficulty in modeling and prediction turns out to be acute at large scales, since the evolution at this scale requires the integration over all smaller scales [Roelvink and Broker, 1993].

The dominant causes of these small scale fluctuations in suspended sediment concentration are unclear and may include instabilities of the bottom boundary layer

[Conley and Inman, 1994; Foster et al., 1995], vortex shedding from megaripples, or coherent turbulent flow structures [Hay and Bowen, 1994]. From a modeling perspective, these small scale processes are difficult to capture. They are driven by various forces including wave, current, and gravity driven flow. There is also significant experimental evidence that flow acceleration, which serves as a proxy for the horizontal pressure gradient in a coastal bottom boundary layer, has an effect on sediment transport [e.g., Hanes and Huntley, 1986; King, 1990; Gallagher et al., 1998; Butt and Russell, 1999; Drake and Calantoni, 2001; Elgar et al., 2001; Puleo et al., 2003].

1.2 Organization

The unifying theme of this project is its association with sediment transport. The first half of the study will attempt to predict the morphology of a real beach in the nearshore with a coupled modeling system. One part of the coupled modeling system is the calculation of the sediment transport. There are several mechanisms, many not yet well understood, that contribute to the movement of sediment in the nearshore. Due to this fact, multiple empirically based parameterizations are incorporated into the sediment transport formulation. The second half of the study will investigate one of these mechanisms that may be vital to accurately predicting sediment transport in the nearshore. Here we will explore the role that pressure gradient forces have on sand grains under shoaling waves compared to that of shear stresses.

Chapter 2 will cover beach evolution on intermediate temporal and spatial scales. Section 2.1 presents an introduction and background on sediment transport models over the past few decades. Section 2.2 describes where the data has come from as well as how the model grid is set up. The individual parts of the modeling system are described in section 2.3 and how they are coupled together. Results are presented in section 2.4.

Finally, a brief discussion and conclusion can be found in sections 2.5 and 2.6, respectively.

The second half of the study on contributions of pressure gradients to sediment transport is presented in chapter 3. A brief background and introduction is given in section 3.1. Section 3.2 takes a closer look at the two stresses. It is here that we examine how at certain wave phases the pressure and shear forces work together to mobilize the bed and explore their interaction under a surface gravity wave. Section 3.3 describes our approach and clarifies the formulation. Results for linear and weakly nonlinear waves are presented in section 3.4. Finally, the paper will close with the conclusion in section 3.5.

CHAPTER 2
A COUPLED MODELING SYSTEM TO PREDICT MORPHOLOGY CHANGES IN THE NEARSHORE

2.1 Introduction

Process-oriented energetics-based total load sediment transport models [Bagnold, 1963] relate sediment transport to the near-bottom flow field and have often been used to predict beach evolution. Bagnold's [1963] arguments are physically reasonable and they seem to capture some of the essential aspects of nearshore sediment transport. The problem is that Bagnold's model yield specific, and thus rigid, parameterizations of some variable small-scale processes. Bagnold sought to parameterize interactions associated with gravitational and near-bed turbulent forces that drive transport under uni-directional river flows. However, several responses of the flow, such as the velocity profiles, the instantaneous bed shear stress, the sediment flux, and the total amount of the mobilized sediment cannot be fully parameterized by a quasi-steady free-stream velocity [Hsu and Hanes, 2004]. The formulas are based on riverine flow that is obviously not the condition that characterizes the nearshore environment.

Since then other researchers have developed similar time-averaged versions of the energetic-based beach profile evolution models [Bowen, 1980; Bailard 1981; Stive 1986; Roelvink and Stive, 1989] using improved parameterization to represent net effects of the small-scale processes more accurately. Several recent studies have tried to compare observed bathymetric changes to predicted cross-shore profile changes from related models [Thornton et al., 1996; Gallagher et al., 1998]. These studies used measured

near-bed velocities to drive the sediment transport model. Both studies concluded that the transport model predicted patterns of offshore transport that were accurate during undertow dominated conditions, where sediment transport was dominated by strong, seaward directed, near-bed, cross-shore mean flow. However, the slow onshore migration observed during low-energy wave conditions was not predicted well.

Detailed hydrodynamic information is hardly ever available in any nearshore environment unless an intensive field study is being conducted. In contrast, wave data is readily available in many coastal environments. Instead of measuring the hydrodynamics from observations, this study will compute the hydrodynamics from measured boundary condition data. The sediment transport is then estimated from the computed hydrodynamics. Plant et al. [2004] found significant predictive skill in a similar approach by tuning several free parameters in the sediment transport model. Plant's study was able to find significant predictive skill for conditions dominated by onshore and offshore transport. However, in order to obtain this skill, it was necessary to allow the model parameters to vary with changing wave conditions. A forward stepping model is sensitive to model parameters, and these parameters should be independent [Plant et al., 2004]. In the present study, the sediment transport parameterization is fixed with one set of model coefficients.

There are many different sediment transport mechanisms, all of which are not included in this model. Therefore the model is limited in that respect. Our model has representation for the depth averaged mean currents, and the combined wave and current boundary layer transports. The model does not yet explicitly include effects contributed by undertow, wave skewness and asymmetry, breaking waves and turbulence, and

surface wave induced pressure gradients. The goal of this work has been to develop a rational framework for a beach morphology model coupled to a wave and mean current model. The precision of knowledge is still lacking pertaining to these unaddressed mechanisms. It is left to the community and future work to fine tune the relative contributions that may be attributable to these neglected mechanisms.

Furthermore, current computer technology requires many approximations in order to simulate for multiple days. To run such extensive simulations you need to run with a 2-D circulation model and a phase averaged wave model. Therefore the undertow, wave skewness, and the turbulence intensities are all parameters that would have to be estimated by some yet-to-be-evaluated methods. As a result, these features were reasonably placed beyond the scope of this stage of the project.

2.2 Observations

Observations used in this study were obtained from the Army Corps of Engineers' Field Research Facility (FRF), located near the town of Duck, North Carolina on a barrier island exposed to the Atlantic Ocean [Birkemeier and Holland, 2001]. We utilized data from the SHOWEX (SHOaling Waves EXperiment) field experiment conducted in the fall of 1999. This data set was chosen for its spatially broad and temporally dense set of bathymetry that extends well beyond the FRF property limits.

2.2.1 Bathymetric Data

Bathymetry was collected by the CRAB (Coastal Research Amphibious Buggy). The CRAB is a 10 meter tall amphibious vehicle, capable of performing surveys to a depth of 8 meters when incident wave heights are less than about 2 meters [Birkemeier and Mason, 1984]. During the SHOWEX experiment, the spatial sampling pattern consisted of shore normal transects, with along-track sample spacing of less than one

meter. The transects typically spanned a 500 meter wide portion of the nearshore and some transects occasionally covered more than 1200 meters in the cross-shore direction. The alongshore spacing of the survey transects were about 45 meters. The extent of the transects in the alongshore, over 2000 meters, is what made this data set most attractive. The two major bathymetric data sets that will be employed in this study are ones that were collected between Oct-26-1999 and Oct-28-1999 and between Nov-05-1999 and Nov-07-1999.

2.2.2 Model Grid

Most previous cross-shore profile evolution models [Bowen, 1980; Bailard, 1981; Stive, 1986; Roelvink and Stive, 1989; Gallagher et al., 1998; Plant et al., 2001] assume alongshore uniformity. This study utilizes the extended data set and grids the entire domain. A domain just north of the pier was chosen to eliminate irregular isobaths around the pier. Furthermore, our wave data is collected just north of the pier as well, so minimal sheltering effects will occur. A constant grid spacing of 5 x 5 meters was chosen with 100 columns and 200 rows. The columns are oriented parallel to the shoreline and the rows perpendicular to the shoreline. Hence, the model domain represents an area of 1000 meters in the alongshore direction and 500 meters in the cross-shore direction. The data were interpolated using the scale controlled methods described by Plant et al. [2002], enforcing smoothness constraints in both the cross-shore and alongshore. A 2-D Hanning filter with an interpolation smoothing scale of 10 meters in the cross-shore and 120 meters in the alongshore was used to generate interpolated profiles.

An important note must be made about the grid rotation. For best model results the domain should be most closely rotated so that the shoreline and/or the sandbar is/are

aligned parallel to the onshore and offshore boundaries. The FRF has tried to do this with their local coordinate system which deviates from the standard latitude/longitude coordinate system. This rotation is approximately 18 degrees counterclockwise from true north. Although this rotation is a best fit to align the entire shoreline parallel with the coordinate system, a new rotation is calculated with the subset grid used in this study. To find the appropriate second rotation, cross-shore trends were calculated and then aligned. The resulting rotation for this data set is an additional slight counterclockwise tilt.

With the alongshore data nearly uniform, a cross-shore trend can be calculated and the data can be filtered. Filtering is done with a spline curve. The filtering will effectively force the unrealistic data, with respect to the cross-shore trend, to have a weighting of zero. It will also force the first derivative to zero at the alongshore boundary. The hydrodynamic model has a few domain requirements. The first requirement is that the gradients be constant on all boundaries. The second requirement of the hydrodynamic model is that there be periodic lateral boundaries. The boundary conditions are enforced with a b-spline curve, which is more sophisticated than a spline curve. The smoothing scale used here is 40 meters in the cross-shore and 150 meters in the alongshore direction. Lastly the hydrodynamics model does not allow bathymetry that is not submerged. Because of this, some interfering must be done in the area of the shoreline. Prediction of the region near the shoreline is not a specific objective although its inclusion is required for boundary conditions on both the sediment transport and the hydrodynamics. This is accomplished by modifying the bathymetry for depths shallower than 40 centimeters and then easing it to a constant depth of 5 centimeters at the shoreline. Experience on this project indicates that this does not significantly influence

the solutions obtained for the beach morphology in deeper water. To address the same constraint of having a submerged bathymetry, the tidal variation is not incorporated into this study but is maintained at mean sea level.

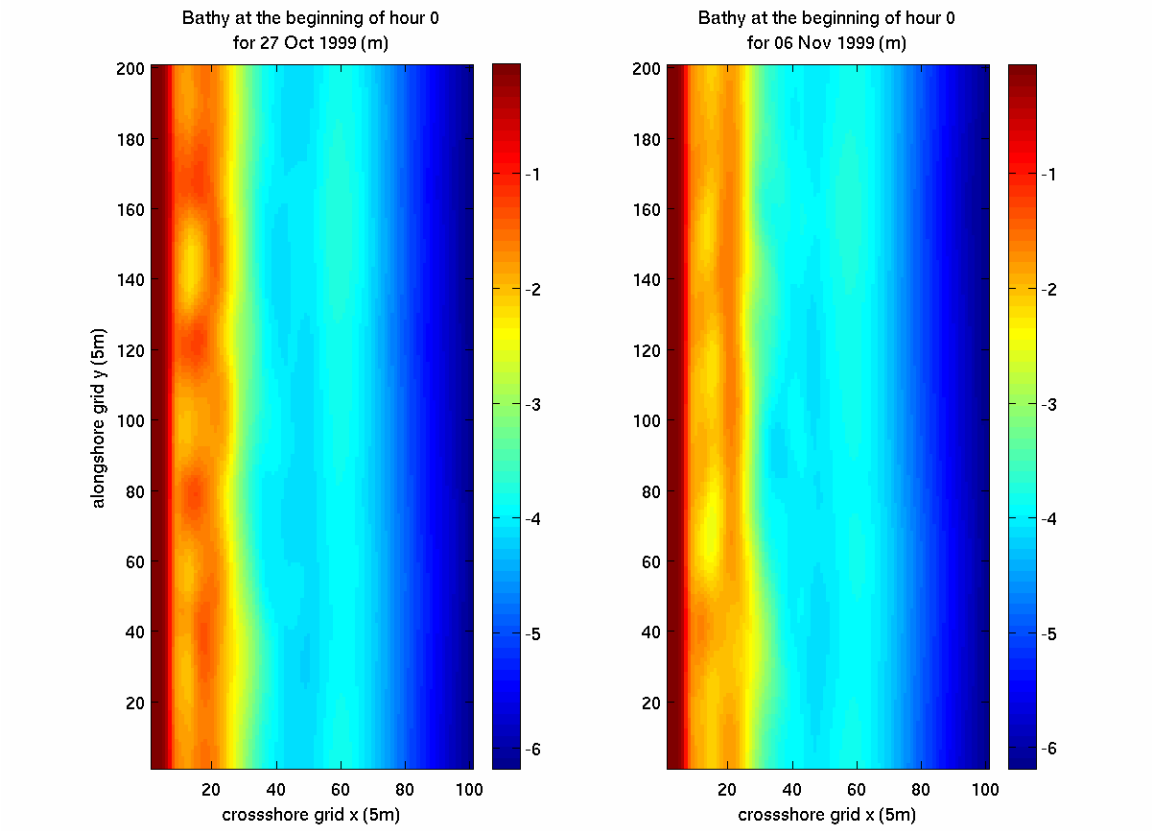

Figure 2-1. Initial bathymetry for Oct. 27, 1999 and Nov 6, 1999.

The two initial bathymetries, which were surveyed in the same approximate area, have some significant differences. The survey on October 27th illustrates a more intricate sandbar system with large amplitude perturbations. This results in a more complex nearshore flow field. In contrast, the survey taken on November 6th exhibits a more linear and shore parallel bar structure.

2.2.3 Wave Data

The wave data was collected using the 8-meter array at the Field Research Facility. The FRF array consists of 15 pressure gauges (collectively referred to as gauge 3111)

mounted approximately 0.5 meters off the bottom. It is located in the vicinity of the 8-meter isobath about 900 meters offshore and to the north of the research pier. Voltage analogs of pressure signals are hard-wired through 10-Hz, fourth-order, Butterworth filters (primarily to eliminate 60-Hz noise) and indicates an accuracy of the pressure equivalent of 0.006 meters of water for wave-induced fluctuations [Birkemeir and Holland, 2001]. These gages supplied estimates of the RMS (root mean squared) wave height, period, and dominant direction at three hour intervals. The dominant wave direction was subsequently rotated to fit our domain orientation. After temporal interpolation to hourly intervals matching the modeling systems computational intervals between bathymetric changes, the wave data supplied by the 8-meter array were applied to the time-varying boundary conditions.

2.3 Model Description

With the initial measured bathymetry and the boundary conditions measured offshore, the wave field and circulation are computed. The computed hydrodynamics then drive a sediment transport formulation. The divergence of the transport is used to predict bathymetric changes. These bathymetric changes are then inserted back to the hydrodynamic model at the subsequent interval with new forcing from the wave model. A resulting coupled modeling system for predicting bathymetric evolution has been developed.

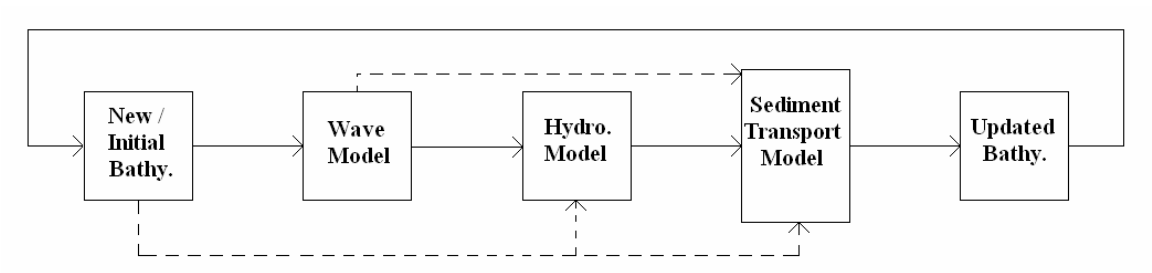

Figure 2-2. Schematic of the coupled modeling system.

The assumption is made that the seabed evolves slowly, such that the feedback of the changing bathymetry and the sediment transport to the hydrodynamic model are only updated on a bathymetric timescale. In other words, the time step taken by the hydrodynamic model (0.075 seconds) is extremely short compared to the morphologic timescale. Therefore, the slowly evolving bathymetry is updated only after intervals of approximately one hour when the hydrodynamics and sediment transport have been integrated forward using the previously computed bathymetry. This eliminates the need for computationally costly time dependant bathymetric updates and new estimates of the wave field at frequent intervals. This assumption is widely accepted and has been used by others experimenting with coupled modeling systems. Gallagher et al. [1998] and Thornton et al. [1996] use a coupled time interval of three hours while Plant et al. [2004] decided on a one hour interval. A time step interval of one hour was chosen for this model, after testing the sensitivity of the results to different time intervals.

Different model durations were investigated briefly. Using measured wave characteristics has limited our runtime scope so that the model would run for a period that would incorporate significant bathymetric changes. For example, to see the response due to storm conditions, the model must simulate through a time period of intense wave conditions. Similarly, if the bathymetric alterations due to a sustained calm wave climate were of interest, the model needs to run throughout many days of calm wave conditions and the adjusted profile needs to be evaluated before any storm conditions occur in the data. As a result, model simulations become very dependent on the measured data. This is complicated due to the fact that the bathymetric data sets are surveyed over multiple days. To minimize error caused by evolving bathymetry during the surveys, the

bathymetric observations were centered at a specific date within the survey and simulations were run from this initial time. This appears to be a valid assumption because surveys can not take place during intense wave conditions and therefore any bathymetric alterations would be minimal from start to finish of the entire survey.

Typical model durations investigated here are approximately two days. Cases were chosen where significant bathymetric changes were large enough to be distinguished from measurement errors. The duration of our simulations were sometimes constrained by numerical instabilities caused by growing shoreline anomalies in the updated bathymetries (section 2.4.1). Others have found a similar range of most advantageous simulated durations. Holland et al. [2000] found that a 5-day interval was close to the optimum prediction interval.

2.3.1 Wave Model

SWAN (Simulating WAves Nearshore), a third-generation stand-alone (phase-averaged) wave model was used to simulate waves over the bathymetry [Booij, 1999]. The offshore RMS wave height was converted to significant wave height and the wave data was submitted to the wave model. For time efficiency, the SWAN model grid spacing in the alongshore direction was increased from 5 meters to 25 meters. The 5 meter cross-shore spacing was preserved. To avoid a shadow zone of waves coming in at an angle, the SWAN input domain must be extended by a factor of three, doubling it in each alongshore direction. This is done by taking the alongshore boundary cross sections (this is also the mean trend cross section) and extending them out to a distance equal to the length of the original domain. The resulting domain is now three times the length of the original.

Many parameters must be determined in order to initialize the wave model. A Gaussian-shaped frequency spectrum was chosen with a spectral width of 0.01 Hz and a directional spreading of five degrees. A constant depth induced wave breaking parameter was also decided on. The proportionality coefficient of the rate of dissipation is 1.0 and the ratio of maximum individual wave height over depth is 0.73.

SWAN has the ability to output a number of different hydrodynamic properties. The one of interest to the hydrodynamics model is the gradient of the radiation stress. For small amplitude waves in irrotational flows, Longuet-Higgins and Stuart [1960] showed that the forcing due to waves is related to the wave radiation stress tensor S. The gradient of the wave radiation stress tensor is conveniently outputted by SWAN as the wave induced force per unit surface area:

$$F_x = -\frac{\partial S_{xx}}{\partial x} - \frac{\partial S_{xy}}{\partial y} \qquad \text{and} \qquad F_y = -\frac{\partial S_{yx}}{\partial x} - \frac{\partial S_{yy}}{\partial y} \quad (2.1).$$

The wave radiation stress tensor is defined as

$$\begin{aligned} S_{xx} &= \rho g \int [n\cos^2\theta + n - 1/2] E d\sigma d\theta \\ S_{xy} &= S_{yx} = \rho g \int n \sin\theta \cos\theta E d\sigma d\theta \quad (2.2), \\ S_{yy} &= \rho g \int [n\sin^2\theta + n - 1/2] E d\sigma d\theta \end{aligned}$$

where n is the ratio of group velocity over phase velocity. The subscripts refer to the direction in which the forces act, where x points offshore and y points in the longshore direction. The gradient of radiation stress must be interpolated back to the original domain before being utilized by the hydrodynamic model.

2.3.2 Hydrodynamic Model

Nearshore circulation can be modeled using the mass and momentum conservation equations that have been integrated over the incident wave timescale and depth. This

model uses a simple forward stepping scheme in time with an interval of 0.075 seconds and the computational grid is set up identically to the bathymetric grid with 5 meter grid spacing. The model uses a third order Adams-Bashforth scheme [Heath, 2002] to calculate the time derivatives and a fourth order compact scheme to calculate spatial derivatives. For an initial condition, the fluid is started from rest $(u(x,y,0) = v(x,y,0) = \eta(x,y,0) = 0)$. A periodicity condition is imposed in the longshore direction. Free-slip or symmetric boundary conditions $(\partial v/\partial x = \partial \eta/\partial x = u = 0)$ are applied at both the shoreline and offshore boundaries using fourth order accurate ghost points. The depth averaged approach is used and assumed to be a reasonable approximation because of the large discrepancy of vertical to horizontal length scales. The vertical depth is under one percent of the horizontal extent of the domain. Time dependant movement of the free surface is included and a fourth order compact filter was added to the flow field in both directions.

Following Ozkan-Haller and Kirby [1999], our computational fluid dynamics (CFD) model solves the two-dimensional, unsteady, Navier-Stokes equations for an incompressible, homogeneous fluid with variable water depth.

$$\begin{aligned}
&\frac{\partial \eta}{\partial t} + \frac{\partial}{\partial x}(\bar{u}d) + \frac{\partial}{\partial y}(\bar{v}d) = 0 \\
&\frac{\partial \bar{u}}{\partial t} + \bar{u}\frac{\partial \bar{u}}{\partial x} + \bar{v}\frac{\partial \bar{u}}{\partial y} = -g\frac{\partial \eta}{\partial x} + \tau_{Fx} - \tau_{bx} \qquad (2.3) \\
&\frac{\partial \bar{v}}{\partial t} + \bar{u}\frac{\partial \bar{v}}{\partial x} + \bar{v}\frac{\partial \bar{v}}{\partial y} = -g\frac{\partial \eta}{\partial y} + \tau_{Fy} - \tau_{by}
\end{aligned}$$

Where $\bar{u}$ and $\bar{v}$ are the depth-averaged mean current velocities in the x and y directions, respectively. Here, η is the phase-averaged water surface elevation above the

still water level, h is the water depth with respect to the still water level, and $d = h + \eta$ is the total water depth.

The hydrodynamic model will simulate unsteady alongshore currents in the surf zone driven by the gradients in radiation stress caused by obliquely incident breaking waves. The incident wave forcing effects are parameterized by τ_{Fx} and τ_{Fy}, and are expressed using the radiation stress formulation by Longuet-Higgins and Stewart [1964]. These terms reduce to

$$\tau_{Fx} = \frac{F_x}{\rho_w d}, \qquad \tau_{Fy} = \frac{F_y}{\rho_w d} \quad (2.4)$$

for straight and parallel contours.

Bottom friction is taken into account through the nonlinear damping terms

$$\tau_{bx} = c_f \frac{\left\langle \left|\vec{U}\right| u \right\rangle}{d}, \qquad \tau_{by} = c_f \frac{\left\langle \left|\vec{U}\right| v \right\rangle}{d} \quad (2.5),$$

where $\langle\ \rangle$ represents a phase-averaged quantity. The total instantaneous velocity vector, $\vec{U}$, includes the cross-shore (u), longshore (v), mean, and oscillatory components of the velocity.

$$\begin{aligned} \vec{U} &= u + v \\ \vec{U} &= (\bar{u} + \tilde{u}) + (\bar{v} + \tilde{v}) \end{aligned} \quad (2.6)$$

Where $\bar{u}$ and $\bar{v}$ are the x and y mean velocity components, respectively and $\tilde{u}$ and $\tilde{v}$ are the x and y oscillatory components of velocity, respectively. The oscillatory component of the velocity can be represented as

$$\begin{aligned} \tilde{u} &= u_o \cos\theta \cos(\omega t) \\ \tilde{v} &= u_o \sin\theta \cos(\omega t) \end{aligned} \quad (2.7),$$

where ω is the radian frequency and u_o is the orbital velocity in shallow water.

$$u_o = \frac{H\sigma}{2}\frac{1}{\sinh(kh)} \quad (2.8),$$

where $\sigma = 2\pi/T$ and T is the peak wave period. The local wave height and wave number are represented by H and k, respectively.

The time average product of the instantaneous velocity magnitude ($\left|\vec{U}\right|$) and the instantaneous alongshore or cross-shore velocity (u or v respectively), found in equation 2.5, are an important component of the circulation model. Fedderson et al. [2000] explains that direct estimation of $\left\langle |\vec{U}|\,u \right\rangle$ requires a more detailed specification of the velocity field than is usually available, so the term $\left\langle |\vec{U}|\,u \right\rangle$ is often linearly parameterized even though linear parameterizations in the mean current frequently are inaccurate because the underlying assumptions (e.g., weak-currents) are violated. Except for the weakest flows, $\left\langle |\vec{U}|\,u \right\rangle$ depends strongly on the mean current and the total velocity variance (oscillatory components of velocity) [Fedderson et al., 2000]. Mean and oscillatory velocities components are the critical constituents to calculating $\left\langle |\vec{U}|\,u \right\rangle$ and subsequently calculating the flow field well.

To solve the difficult formulation of $\left\langle |\vec{U}|\,u \right\rangle$, we use the nonlinear integral parameterization method. To do this, one must integrate over the wave period at every time step.

$$\begin{aligned}
\left\langle |\vec{U}|\,u \right\rangle &= \frac{1}{T}\int_T [u_o{}^2\cos^2(\omega t) + 2u_o\cos(\omega t)(\bar{u}\cos\theta + \bar{v}\sin\theta) + \bar{u}^2 + \bar{v}^2]^{1/2}[\bar{u} + u_o\cos\theta\cos(\omega t)]dt \\
\left\langle |\vec{U}|\,v \right\rangle &= \frac{1}{T}\int_T [u_o{}^2\cos^2(\omega t) + 2u_o\cos(\omega t)(\bar{u}\cos\theta + \bar{v}\sin\theta) + \bar{u}^2 + \bar{v}^2]^{1/2}[\bar{v} + u_o\cos\theta\cos(\omega t)]dt
\end{aligned} \quad (2.9)$$

Following McIlwain and Slinn [2004], these integrals are evaluated numerically using Simpson's rule [Hornbeck, 1975] with 16 intervals. The above integrals require significant computational effort to evaluate and, in our case, will increase the computational time by a factor of three. If one is not willing to sacrifice this computational time, then the less accurate linear parameterization method should be used.

The nonlinear damping terms τ_{bx} and τ_{by} are the free parameters in the model and truly are a source of uncertainty. The friction coefficient parameter, c_f will effectively control the nature of the resulting motion. Depending on the values of the friction coefficient, fully developed fluctuations can behave in a variety of ways ranging from equilibrated, small-amplitude fluctuations to energetic, random fluctuations involving strong vorticies [Slinn et al., 1998]. Ozkan-Haller and Kirby [1999] and Slinn et al. [1998], both found that a stronger mean current, more energetic fluctuations in the velocities, faster propagation speeds, and more energetic vortex structures result as the friction coefficient c_f is decreased. The flow field exhibits shear instabilities of the longshore current due to the reduction of this term and results in unsteady longshore progressive vortices. These shear instabilities are found to induce significant horizontal mixing in the surf zone and affect the cross-shore distribution of the mean longshore current [Ozkan-Haller and Kirby, 1999]. McIlwain and Slinn [2004] establish for the nonlinear integral parameterization method used here, the best agreement with observed data came from a c_f value of 0.003.

The effect of lateral mixing due to turbulence and the dispersive three-dimensional effect of the vertical fluctuations in the current velocities [Svendsen and Putrevu, 1994] have been neglected and left out of the shallow water equations. Ozkan-Haller and Kirby

[1999] found, for reasonable mixing coefficients, that the mixing induced by the instabilities in the flow dominates over mixing due to eddy viscosity terms, which include the effects of turbulence and depth variation in the current velocities. They also found that the presence of the shear instabilities and the associated momentum mixing actually tends to suppress momentum mixing due to the eddy viscosity terms.

2.3.3 Sediment Transport Model

For steady, two-dimensional unidirectional stream flow, Bagnold [1963] utilized an energetics-based sediment transport model assuming that the sediment is transported in two distinctly different modes. Sediment transport as bedload occurs via bed shear stress from the fluid flow plus the downslope contribution of gravity, while sediment transport as suspended load occurs via turbulent diffusion by the stream fluid. The total immersed weight sediment transport rate, i, can be represented as [Bagnold, 1966]

$$i = i_b + i_s = \left(\frac{\varepsilon_b}{\tan\phi - \tan\beta} + \frac{\varepsilon_s}{(W/\bar{u}) - \tan\beta}\right)\omega \quad (2.10),$$

where subscripts b and s refer to bedload and suspended load, respectively. The parameter β is the local bed slope and ϕ is the angle of repose which is taken to be 28° [Julien, 1998]. The percent of power used for bedload and suspended load is represented with the efficiency factors ε_b and ε_s. Following Thornton et al. [1996], $\varepsilon_b = 0.135$ and $\varepsilon_s = 0.015$. The rate of energy production of the stream ω, is equal to the product of the time-averaged bottom stress τ and the mean free stream velocity,

$$\omega = \tau\bar{u} \quad (2.11).$$

The shear stress at the bed can be represented by

$$\tau = \rho_w C_f \left|\bar{u}\right|\bar{u} \quad (2.12)$$

Inserting equation 2.12 into equation 2.11 yields

$$\omega = \rho_w C_f \left|\overline{u}\right|^3 \quad (2.13)$$

where ρ_w is the density of water. Mean and fluctuating velocity components contribute to the nonlinear term $\left|\overline{u}\right|^3$, just as described in section 2.3.2.

The steady-flow transport equation is then extended to include oscillatory flows as well as steady flows [Bailard, 1981; Bailard and Inman, 1981]. The contribution of the longshore bottom stress is also included. The resulting time averaged immersed weight suspended sediment transport rate, Q, is

$$\begin{aligned} Q_x &= K_b \rho_w \left(\left\langle |\vec{U}|^2 u \right\rangle - \frac{\tan\beta_x}{\tan\phi}\left\langle |\vec{U}|^3 \right\rangle\right) + K_s \rho_w \left(\left\langle |\vec{U}|^3 u \right\rangle - \frac{\epsilon_s}{W}\tan\beta_x \left\langle |\vec{U}|^5 \right\rangle\right) \\ Q_y &= K_b \rho_w \left(\left\langle |\vec{U}|^2 v \right\rangle - \frac{\tan\beta_y}{\tan\phi}\left\langle |\vec{U}|^3 \right\rangle\right) + K_s \rho_w \left(\left\langle |\vec{U}|^3 v \right\rangle - \frac{\epsilon_s}{W}\tan\beta_y \left\langle |\vec{U}|^5 \right\rangle\right) \end{aligned} \quad (2.14)$$

with the units kg/s^3 and $\langle\ \rangle$ represents a time average over many wave periods. The coefficients K_b and K_s [Gallagher et al., 1998] are

$$K_b = \frac{\rho_w}{\rho_s - \rho_w} c_f \frac{\epsilon_b}{\tan\phi} \qquad \text{and} \qquad K_s = \frac{\rho_w}{\rho_s - \rho_w} c_f \frac{\epsilon_s}{W} \quad (2.15),$$

where ρ_s is the density of the sediment. K_b is dimensionless while K_s has the dimensions of s/m. The coefficient of friction c_f is the same as referred to earlier in section 2.3.2. Just as in the hydrodynamics model (section 2.3.2), the product $\left\langle |\vec{U}|u \right\rangle$ is solved using the nonlinear integral parameterization method integrating numerically with Simpson's rule.

The sediment fall velocity is represented by W. The effect of grain size is handled only explicitly via the fall velocity. The offshore sands are often finer than the sand in the nearshore region and must be represented that way. Plant et al. [2004] found that the highest prediction skill was achieved by using a temporally constant but cross-shore variable distribution of sediment fall velocities.

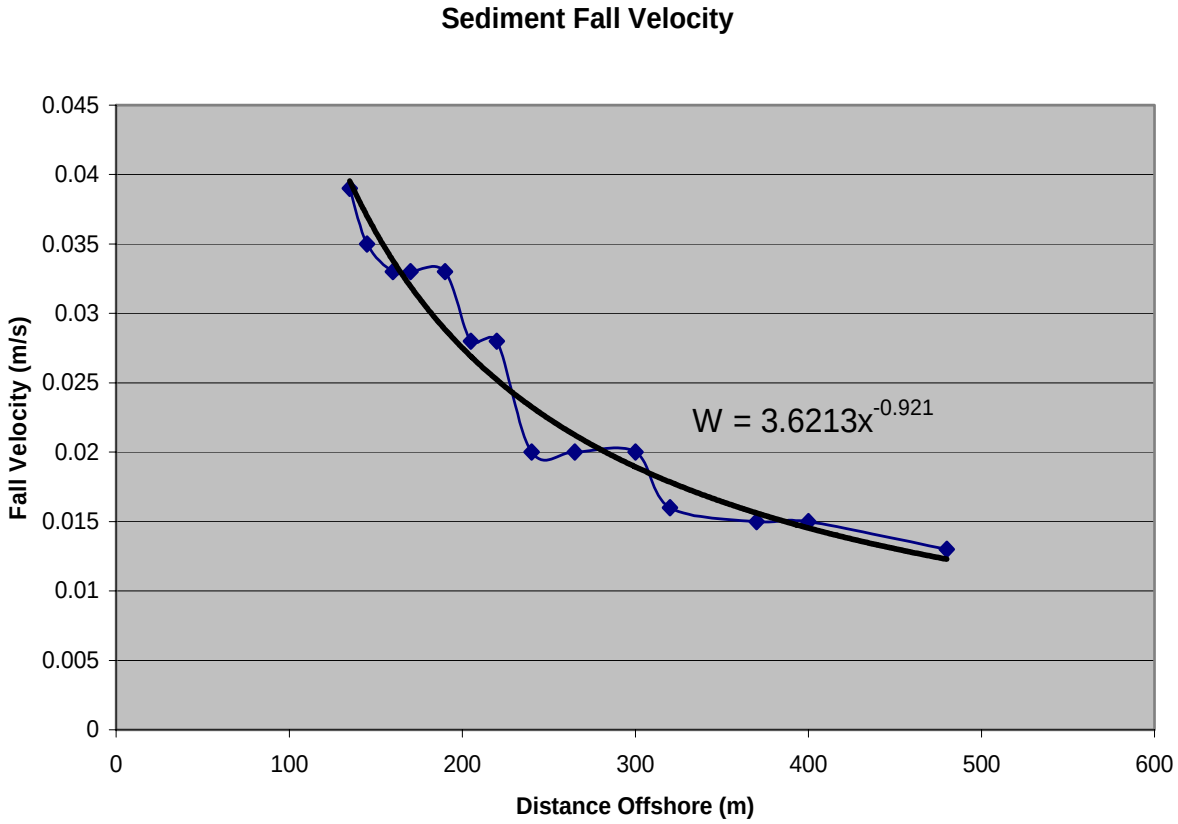

Figure 2-3. Fall Velocity as a function of offshore distance.[1]

The bed evolution depends on the divergence of the time averaged transport rate, Q. Mass conservation in both the cross-shore and alongshore directions yields

$$\frac{dh}{dt} = \frac{1}{\Lambda g \rho_s}\left(\frac{dQ_x}{dx} + \frac{dQ_y}{dy}\right) \quad (2.16).$$

[1] Sediment fall velocity as a function of cross-shore location (following Sleath 1984) from data collected in 1984-1985 at the FRF [Stauble 1992]. A power series trendline is used to fit the data.

Assuming the density of sediment packing is constant, Λ is the packing factor and taken to be 0.7 [Thornton et al., 1996]. The divergence of the time averaged transport rate is calculated at the end of each coupled time interval. The bathymetry can now be updated for the subsequent time interval.

$$h_{new} = h_{old} + dh \quad (2.17)$$

The constraint of having a submerged bathymetry is still enforced after the bathymetry is updated. Therefore, to conserve mass, any bathymetry that emerges beyond the 5 centimeter depth contour will be scoured back to 5 centimeters and the remaining bathymetry at that node will be added to the closest cross-shore node in the offshore direction. This seems to only happen at the shoreline and may even represent shoreline accretion. But as mentioned before, prediction of the region near the shoreline is not a specific objective of this study.

Extra filtering was incorporated to the sediment flux as well as the divergence of the sediment flux at the end of each coupled time interval to reduce any irregular isobaths primarily at the shoreline. With a fixed set of parameters in the hydrodynamic and sediment transport model, the calculations can become less stable when there is an oddity in the bathymetry especially near a boundary like the shoreline. Therefore this extra filtering was incorporated with a fourth order compact filter in both directions. While this technique was introduced for model stability issues, we note that this could even represent horizontal smoothing attributable to turbulent diffusion at the bed. Filtering may help our model stay numerically stable but it will consequently decrease the net localized accretion or erosion of small scale features.

2.4 Results

Two model simulations were run in this study. One from the bathymetric data gathered in the region of October 27th, 1999 (hereinafter OCT27) and another from the bathymetric data surveyed around the date of November 6th, 1999 (hereinafter NOV6). The two simulations were started from approximately the same location area with each of their respected initial bathymetries (Section 2.2.2). They were stepped forward in time with measured wave data. The wave data varies quite dramatically between the two simulations.

OCT27 (Fig. 2-4) represents a calmer wave climate period. While the first few hours are a bit stormy, it then calms down with wave heights hovering around 1 meter as a long South-East swell enters the nearshore.

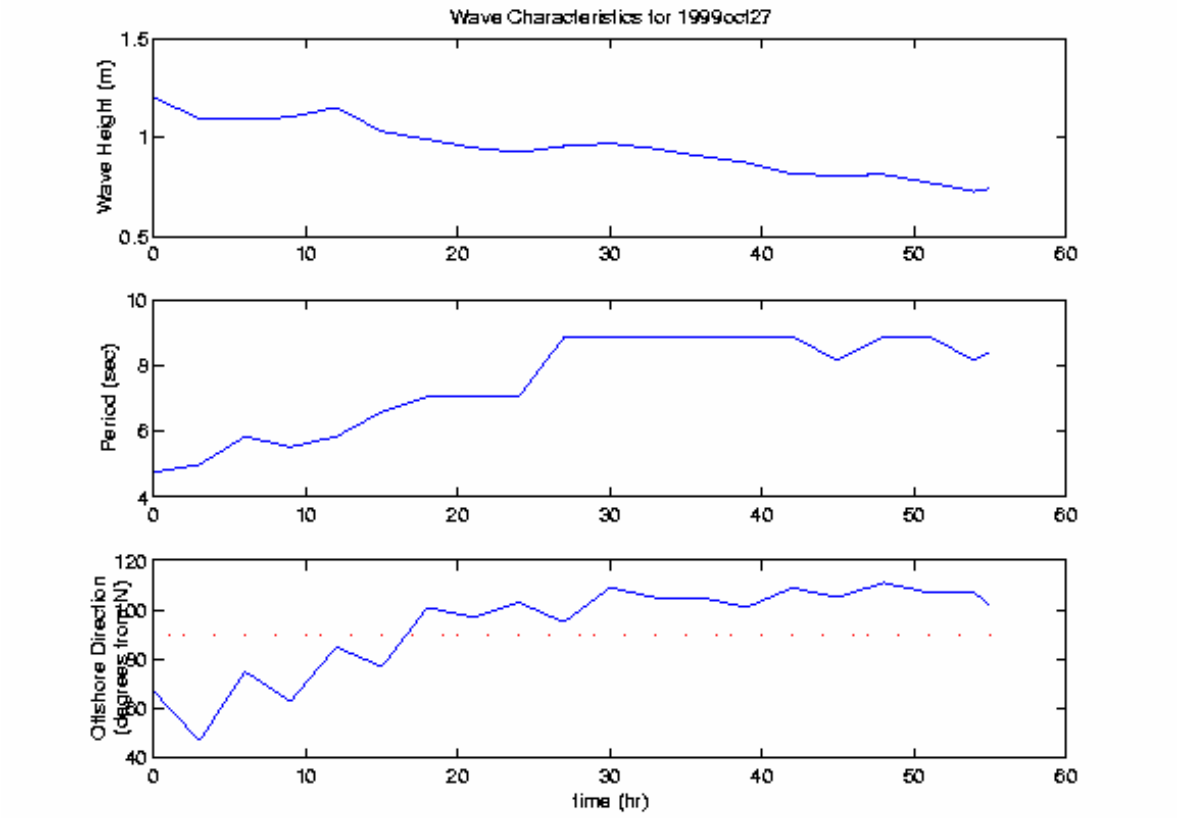

Figure 2-4. Wave characteristics for October 27, 1999.

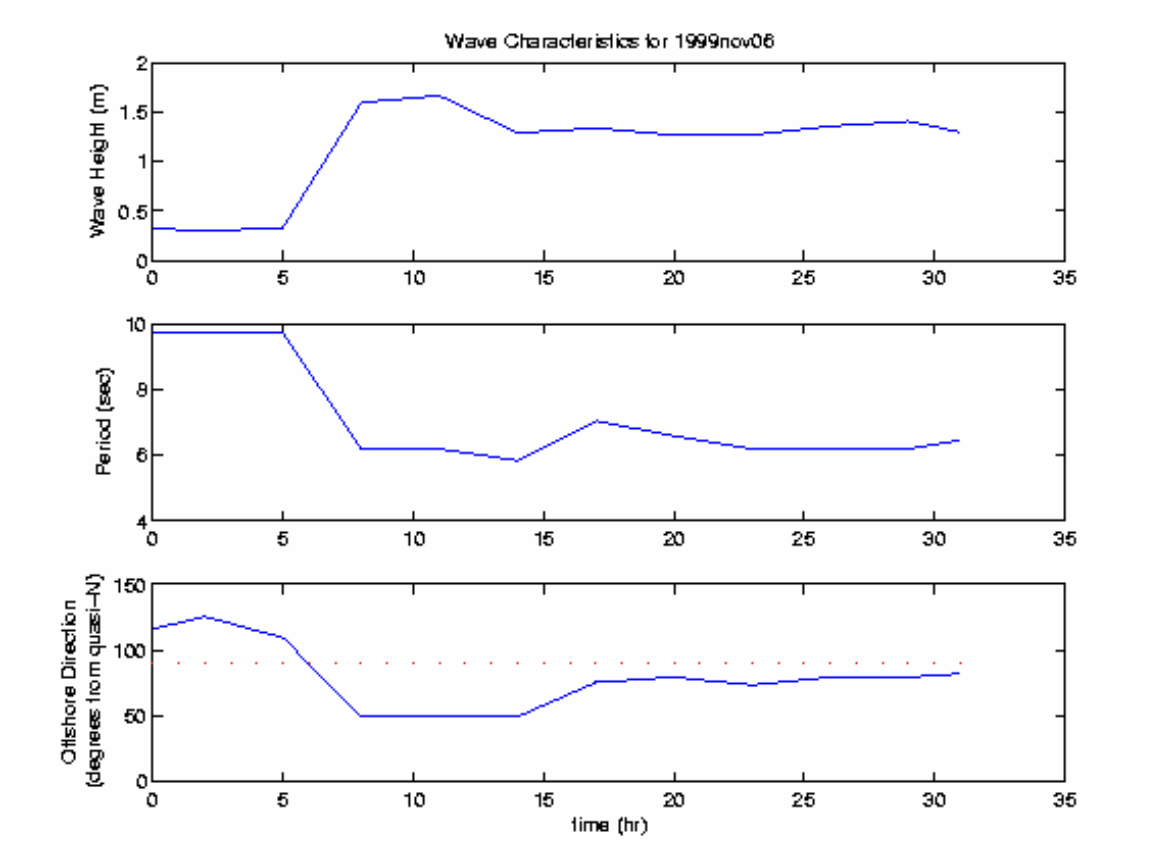

Figure 2-5. Wave characteristics for November 6, 1999.

Conditions were quite different for the NOV6 (Fig. 2-5) simulation. The first few hours of the simulation consist of waves with a long period approaching from the south-east but around hour 5 the wave climate dramatically strengthens. Waves begin to approach from the north-east with wave heights exceeding 1.5 meters and wave periods around 6 seconds. The performance of the model for the two simulations is more interesting because the initial bathymetries and the wave climates significantly differ.

2.4.1 October 27th Simulation

The intricate initial bathymetry (Sec. 2.2) causes the flow field as well as the sediment transport to be quite complex for this simulation. The flow field and the transport also have a strong correlation with each other.

When the waves are entering the nearshore from a large enough angle away from shore normal (+/- 10 degrees), a recognizable alongshore current can be identified. This is evident from time series of the alongshore and cross shore velocities at a single point in the flow field.

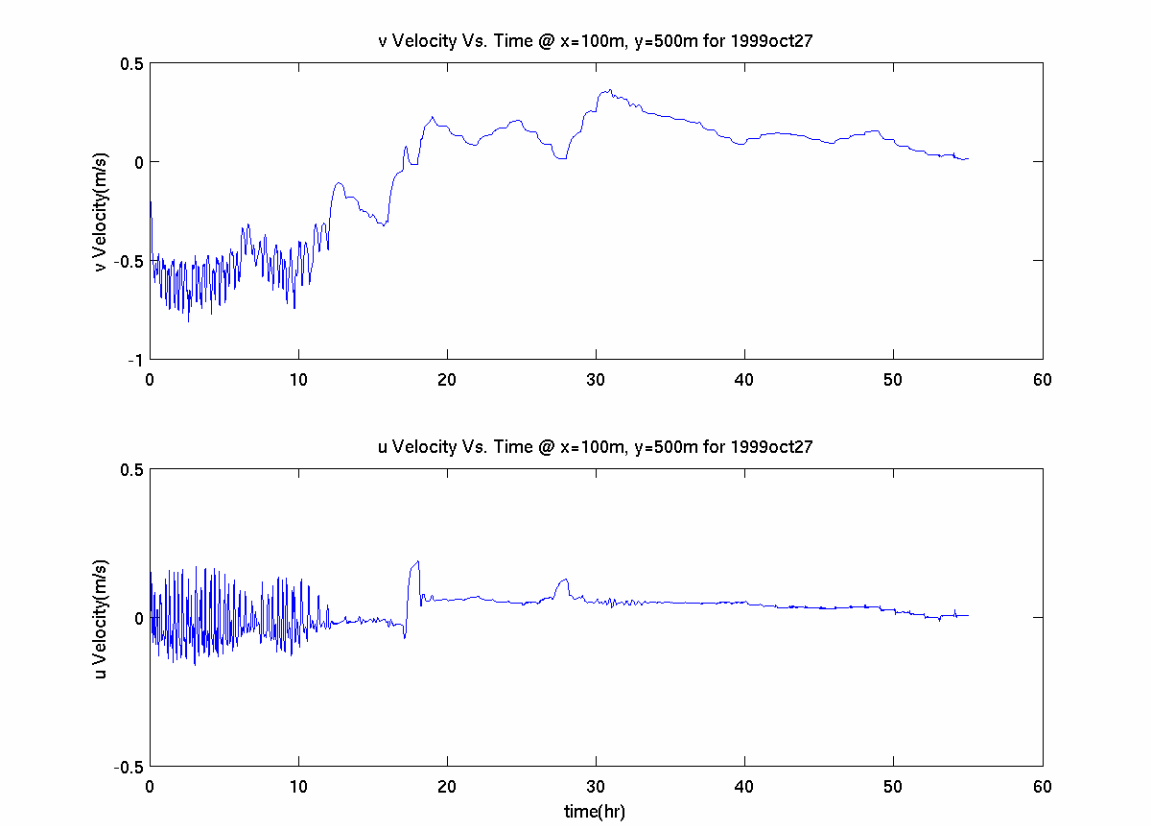

Figure 2-6. Time series of the cross shore and alongshore velocities for October 27th.

The point chosen to record this velocity time series is located 100 meters offshore and 500 meters from the bottom of the grid. This point was selected because it is located close enough to the shore to track evidence of an alongshore current. Notice the cross shore velocity (u) time series will oscillate around 0 m/s and gives an indication of how unsteady the flow is. On the other hand, the alongshore velocity (v) time series indicates the alongshore direction of the flow. The correlation of wave direction and alongshore

velocity direction can be seen as well as the unsteadiness of the cross shore velocity during the larger wave periods.

The complex bathymetry causes the flow to exhibit a meandering around the perturbations in the sandbar similar to that reported by Slinn et al. [2000]. This is evident by looking at a stream function field of the alongshore velocity overlaying the existing bathymetry.

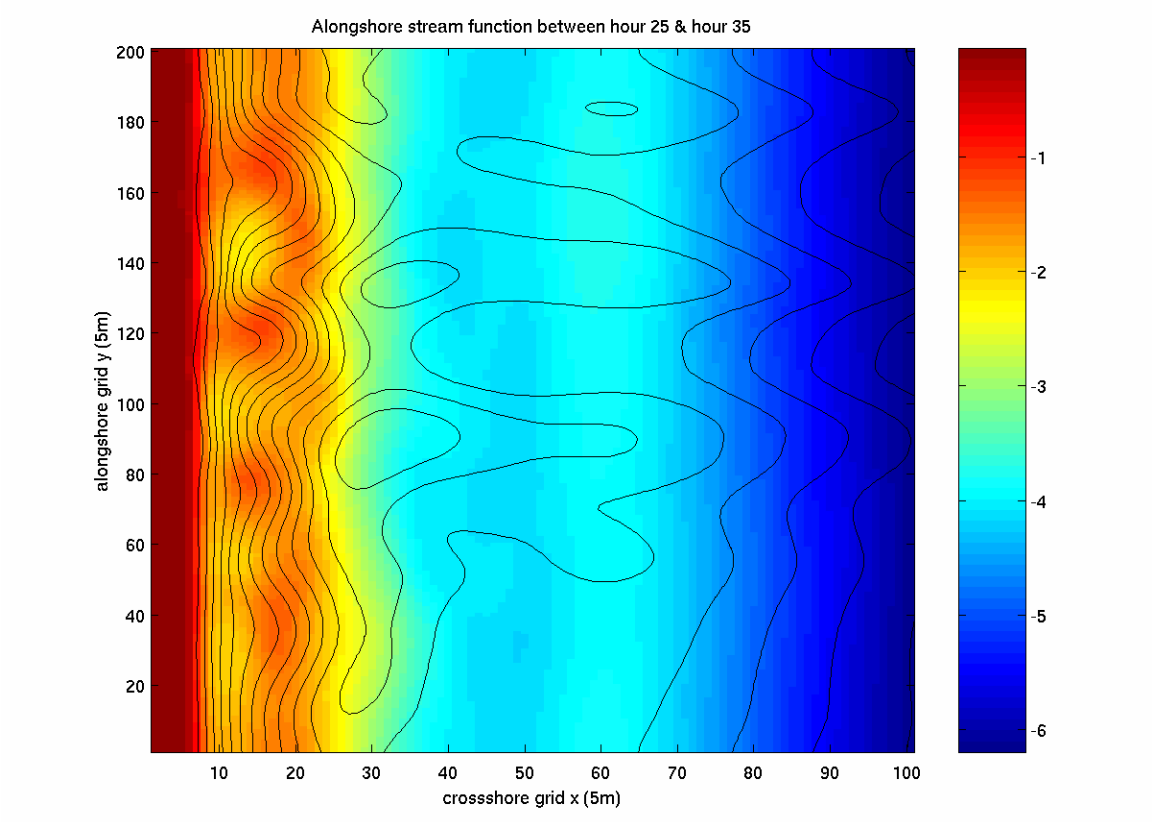

Figure 2-7. Time averaged alongshore stream function for October 27th.

The stream function of the time averaged flow was calculated for a ten hour interval within the simulation. It is averaged from the beginning of hour 25 to the end of hour 34. During this time the waves are approaching from a south-east direction. Therefore the stream lines run from the bottom of the grid to the top. Note the more narrow spacing between the stream lines, denoting a stronger flow, in the nearshore. As you can see, the

current senses the bottom and seems to curve around the high points. The flow field will continue to bend around these perturbations as long as the waves approach the shore with the same angle and height.

The sediment transport is also correlated with the meandering of the alongshore current.

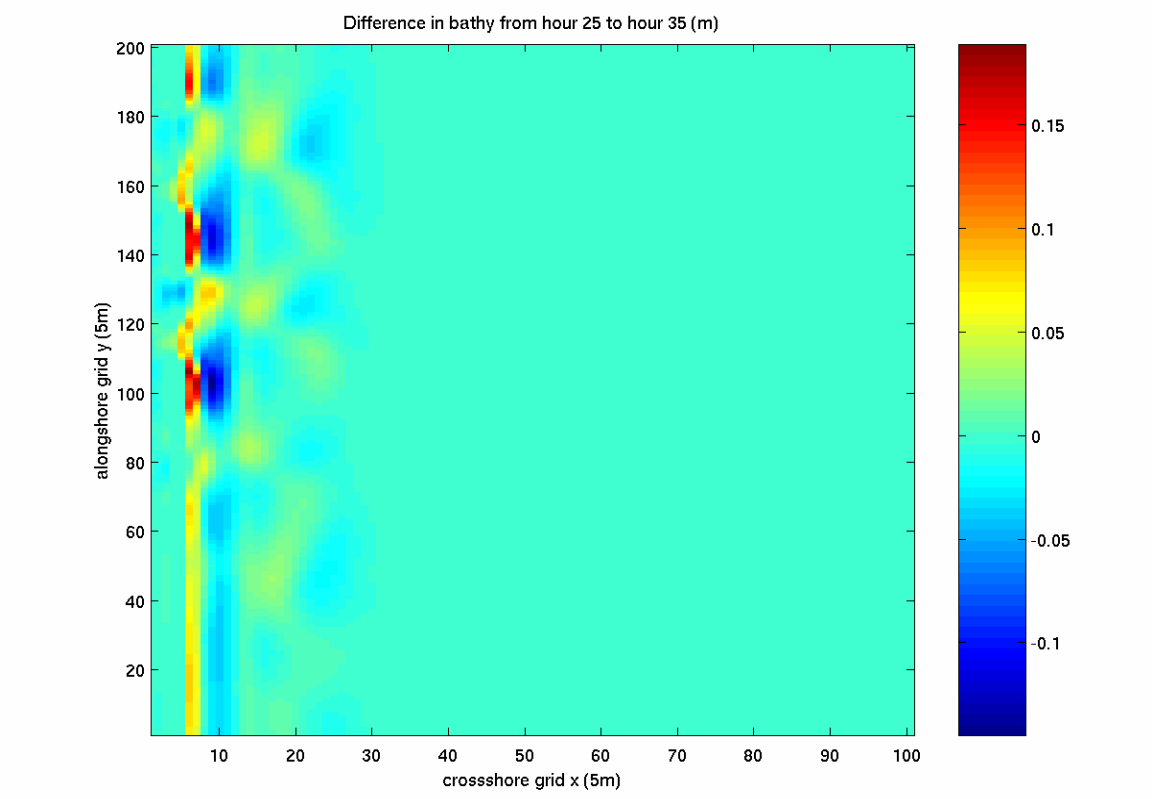

Figure 2-8. Bathymetric change from hour 25 to hour 35.

Figure 2-8 shows the change in bathymetry recorded for the same simulated time span as the alongshore stream function above (Fig. 2-7). Looking at the bathymetry change away from the shoreline in the sandbar region (around 100m from the left edge of the grid), one can detect a sort of meandering of the sediment transport as well. A correlation is evident when compared to the stream function (Fig. 2-7). When the time averaged alongshore current is headed offshore, it is accompanied by an offshore transport. Conversely, when the stream turns back shoreward, an onshore sediment transport can be seen. Also note

that the onshore transport regions are of stronger magnitude. This is likely related to the contribution from the wave velocities to the total velocity vector. When the principle wave axis and the mean current vector are aligned, the nonlinear product of the total velocity squared or cubed is much larger then when the two velocity components are not collinear. Figure 2-9 shows that local wave heights are also larger in these same regions.

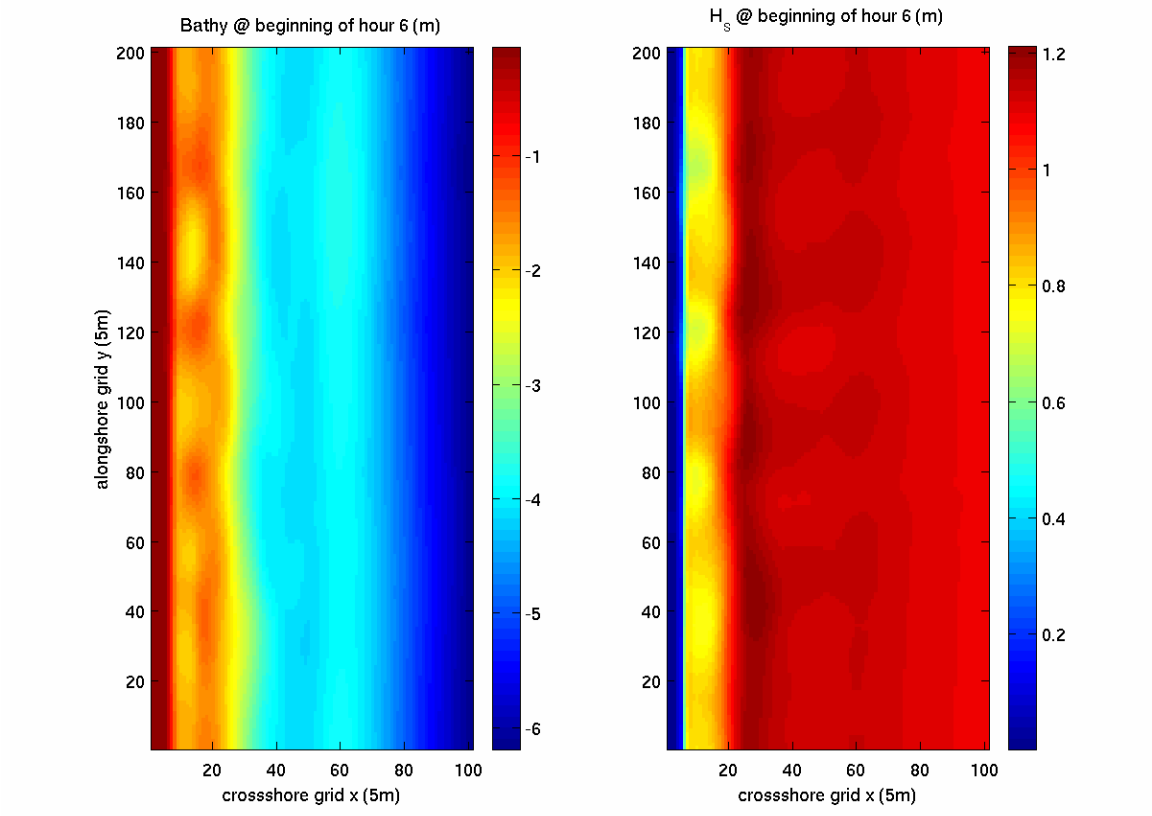

Figure 2-9. Wave focusing around bathymetry for October 27th.

It is also apparent that the perturbations in the bathymetry are causing wave focusing. This is a significant effect and often observed in nature but it also causes additional complications for this study. The focusing creates large pockets of energy at the shoreline. Consequently, immense scouring and erosion can be found at these points. These shoreline perturbations can tend to grow and subsequently result in the flow becoming numerically unstable. Various methods to alleviate these difficulties were

implemented with varying degrees of success. As stated above, prediction of the region near the shoreline is not our main specific objective although its inclusion is necessary for providing boundary conditions for both the transport divergence and the hydrodynamic formulations. Our main focus is on bar migration. Because of problems near the shoreline, however, our model simulation runs are limited to the duration until the hydrodynamics become numerically unstable around the odd and jagged shoreline bathymetry. When a fixed set of hydrodynamic and transport parameters are implemented, it is difficult for the model to cope with either variations in the wave climate or, in our case, peculiarities of the formulations in very shallow water near the boundary conditions. Shoreline stability and more accurate shoreline transformation is a future goal of this continuing study. A number of potentially fruitful avenues are open to further investigation. One that will be explored below is simply to make the shoreline static and let the remaining bathymetry evolve.

The net bathymetry change exhibits a similar pattern of sandbar meandering and jagged cuspate features near the shoreline (Figure 2-10). These concentrated sharp shoreline perturbations are found directly behind the sandbar crests and are a direct effect of wave focusing. The magnitude of the sediment transport is relatively small; only about 20 cm of vertical change over 55 hours in the sandbar region. This may be realistic due to the calm wave climate but in our judgment more likely to be an underestimate. The next bathymetric survey occurred approximately 200 hours later and we were unable to integrate the modeling system forward to that duration because of the shoreline stability. This made it impossible to make direct comparisons of the model hindcasts with survey data.

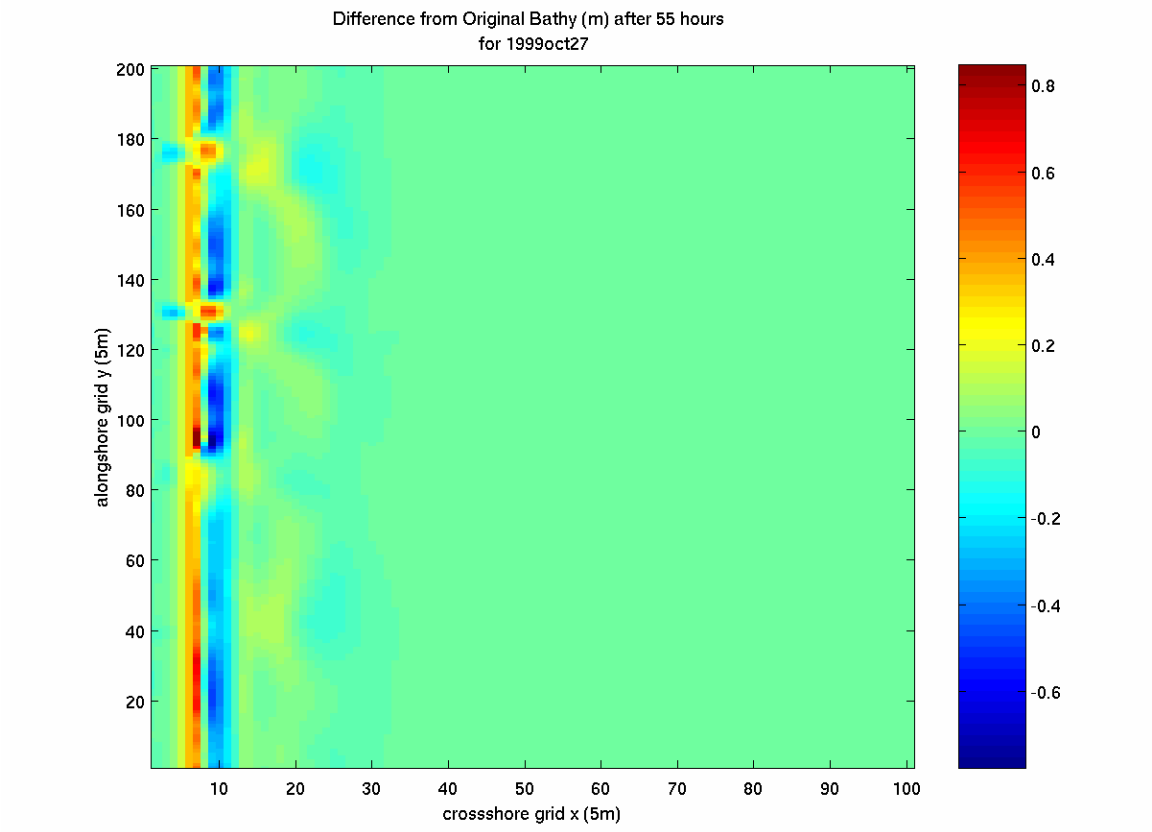

Figure 2-10. Difference in bathymetry from original for Oct 27th.

As mentioned above, a simulation was run holding the shoreline in place and letting the rest of the bathymetry evolve. This allows us to focus in on the transport magnitudes specifically in the sandbar region. But note, variation of the shoreline that may indeed happen and the consequential effects to the rest of the bathymetry are not included. A comparison of the two different approaches for similar time intervals reveal quite similar results but with the magnitude of the static shoreline approach slightly higher due to less filtering needed. Figure 2-11 shows the magnitudes of transport in the bar region for the same time interval as Figure 2-10 but with a static shoreline region.

In the regions where sediment is moving onshore, some shoreward advancement of the sandbars can be seen, but only minimally.

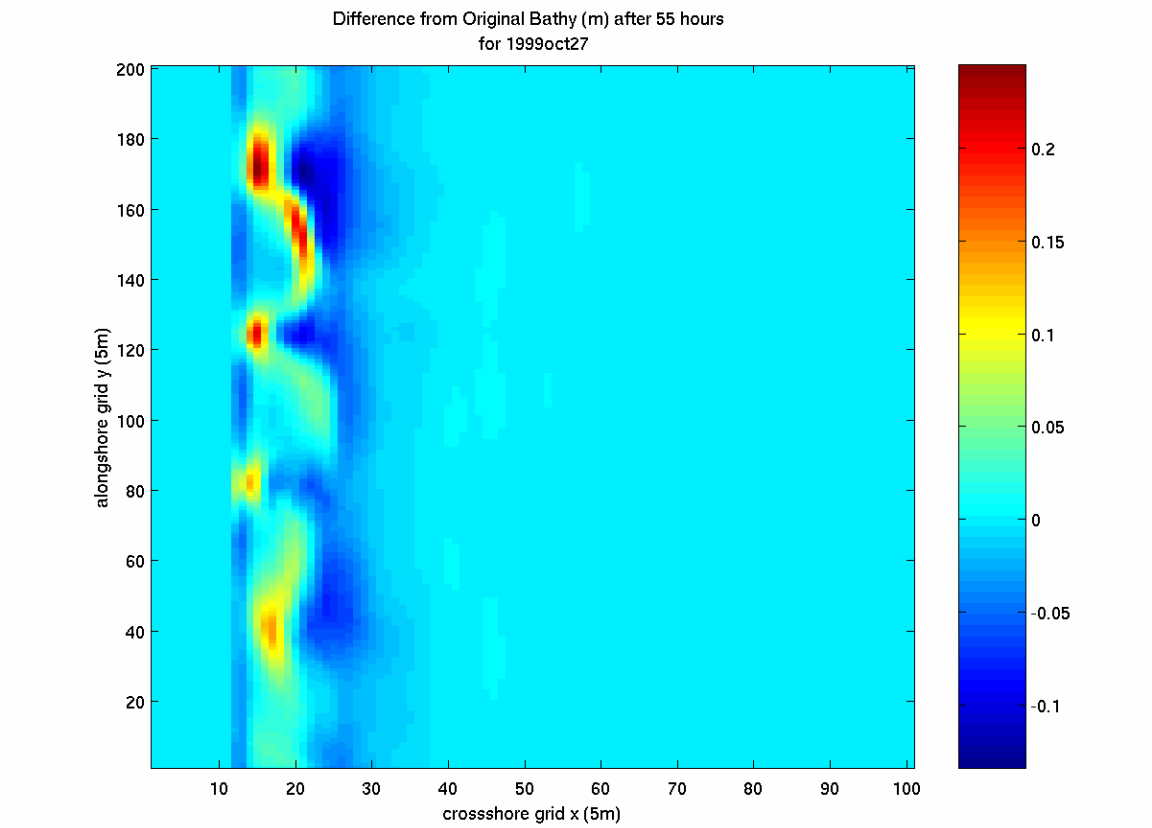

Figure 2-11. Difference in bathymetry for October 27th with the shoreline held static.

The sediment transport appears to be building the bar more than moving it shoreward. This is even evident where there is a trough in the bar and net offshore transport is detected. The net sediment accretion is enclosed within sediment depletion on both the shoreward and offshore edges. While these magnitudes seem smaller than expected, the transport shape and directions appear reasonable and consistent with the model formulation.

Holding the shoreline static also allows us to run our simulation further in time. A simulation of 130 hours was completed. Similar wave conditions were observed for the remaining 75 hours; relatively small waves (less than a meter) coming from the south east. Figure 2-12 shows the same general transport shape with larger magnitudes.

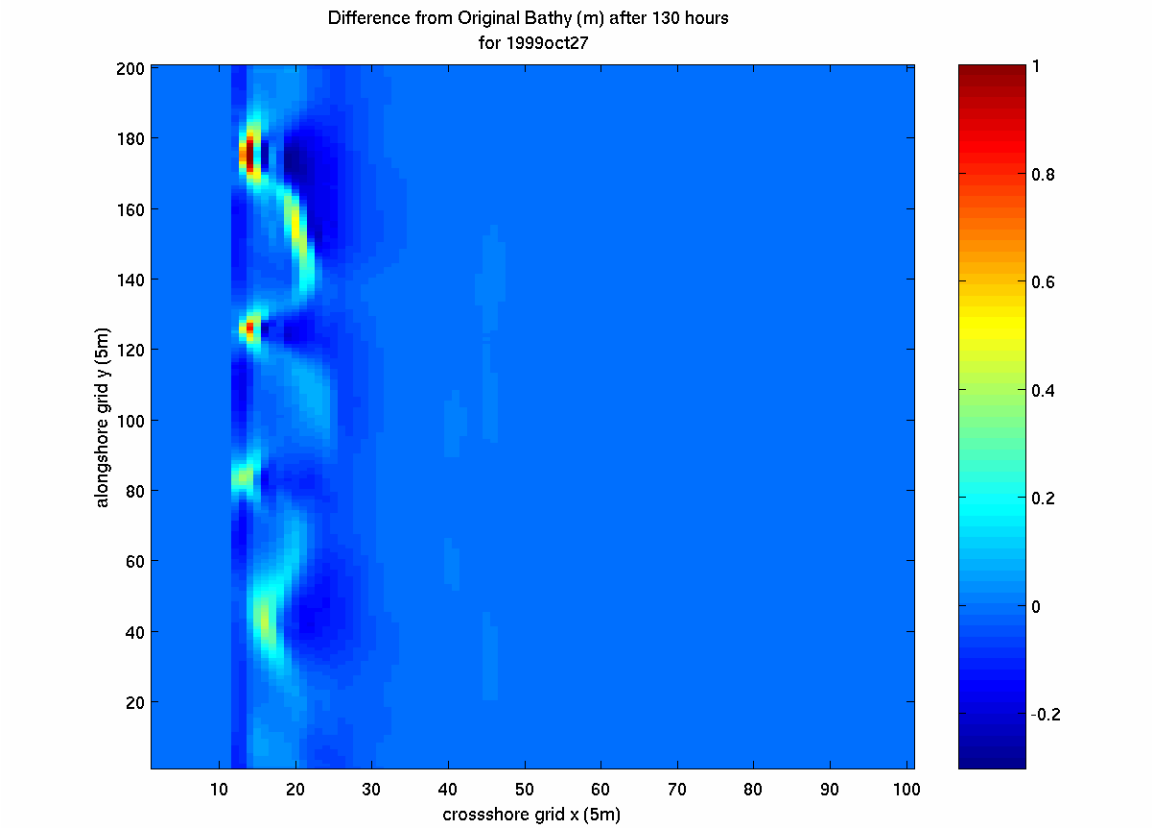

Figure 2-12. Difference in bathymetry for October 27th after 130 hours with the shoreline held static.

The 130 hour simulation (just over 5 days) eventually incurred similar stability problems as the variable shoreline simulations. Instead of sharp cuspate features appearing and growing at the shoreline, the sandbar ultimately became jagged and caused the model to break down numerically. Therefore the model was never able to run a full 10 day simulation. Even after the 5 day simulation it is apparent that the sandbar evolution is not desirable. One would expect the sandbar perturbations introduced in October 27th survey to smooth out to the linear bar exhibited by the November 6th survey (Figure 2-1). This is obviously not the case from Figure 2-12. Here again, the bar seems to be building rather than smoothing out.

2.4.2 November 6th Simulation

The initial bathymetry for NOV6 (Sec. 2.2) demonstrates a much more linear sandbar than OCT27's bathymetry. Furthermore, the wave climate and circulation is much more intense (Fig. 2-5). This is evident by the time series of the alongshore and cross shore velocities at the same point in the flow field.

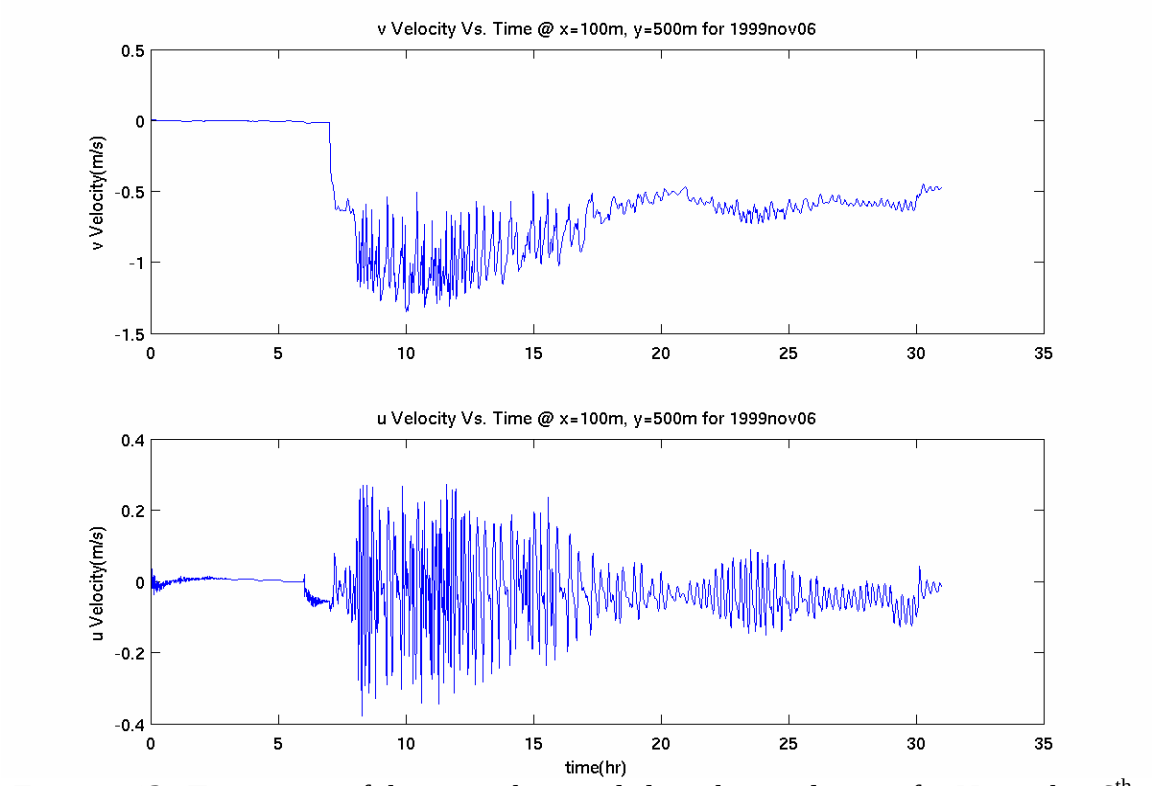

Figure 2-13. Time series of the cross shore and alongshore velocities for November 6th. The magnitude of the alongshore velocity is clearly more powerful and more unsteady in the cross shore direction than for the OCT27 simulation (Fig. 2-6). It is easy to see the unsteadiness when the vorticity fields are compared.

The stream function is calculated during a 10 hour period of 1.5 meter waves coming from the north-east (so a particle would follow the stream line from the top of the grid to the bottom).

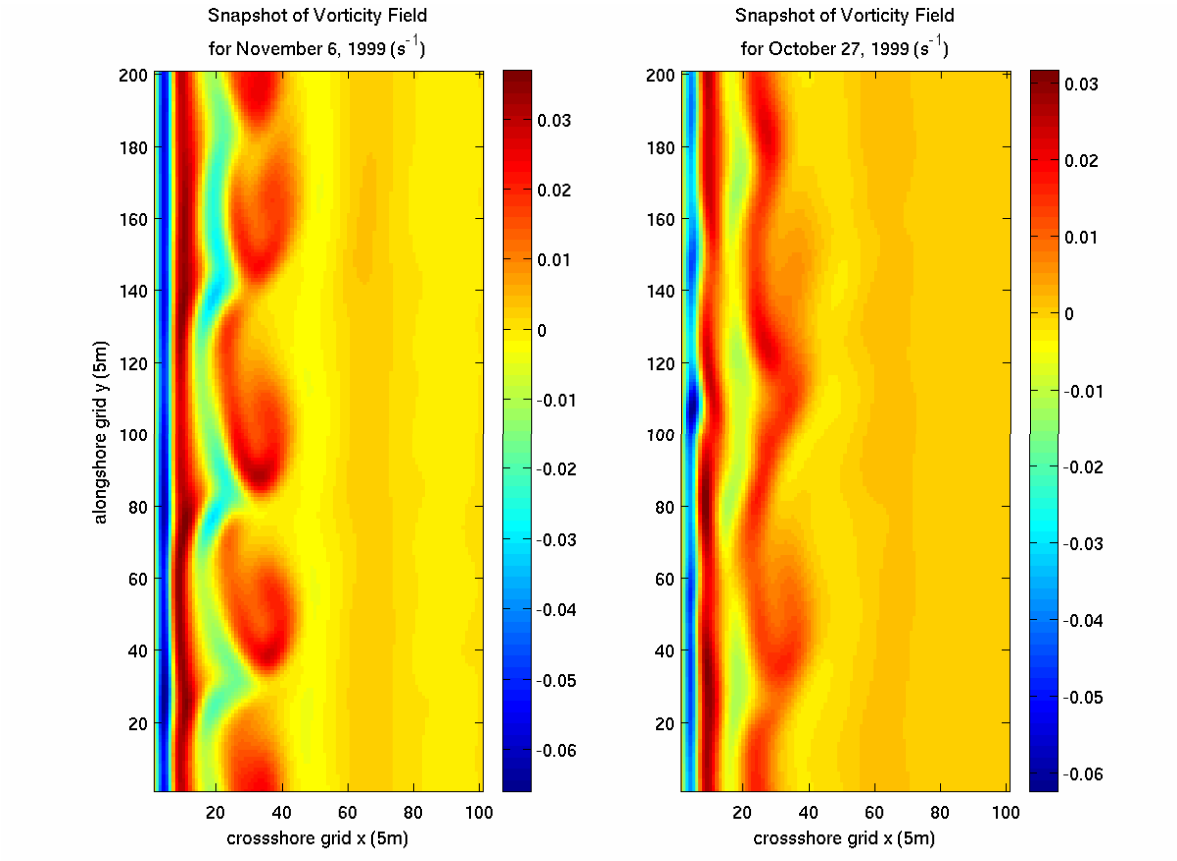

Figure 2-14. Snapshot of the vorticity fields.

The proximity of stream lines within the sandbar region show the relatively much stronger alongshore current with respect to the OCT27 simulation (Figure 2-7). Although there seems to be quite a bit of vortex shedding, the alongshore mean current flows in a very linear fashion parallel to the sandbar.

Wave focusing and shoreline concentration, as stated above, appear to be a problem in this simulation as well. While the initial sandbar is nearly linear and parallel to the shoreline, it does have a distinct trough and high point located about 200 meters from the bottom of the grid. This may be easier to see in a 3-dimensional bathymetry as shown in Figure 2-16. Similar to the first simulation, the waves focus here, as well as at the northern portion of the grid, and subsequently the shoreline perturbations eventually

cause the circulation model to become numerically unstable near the shoreline after 31 hours.

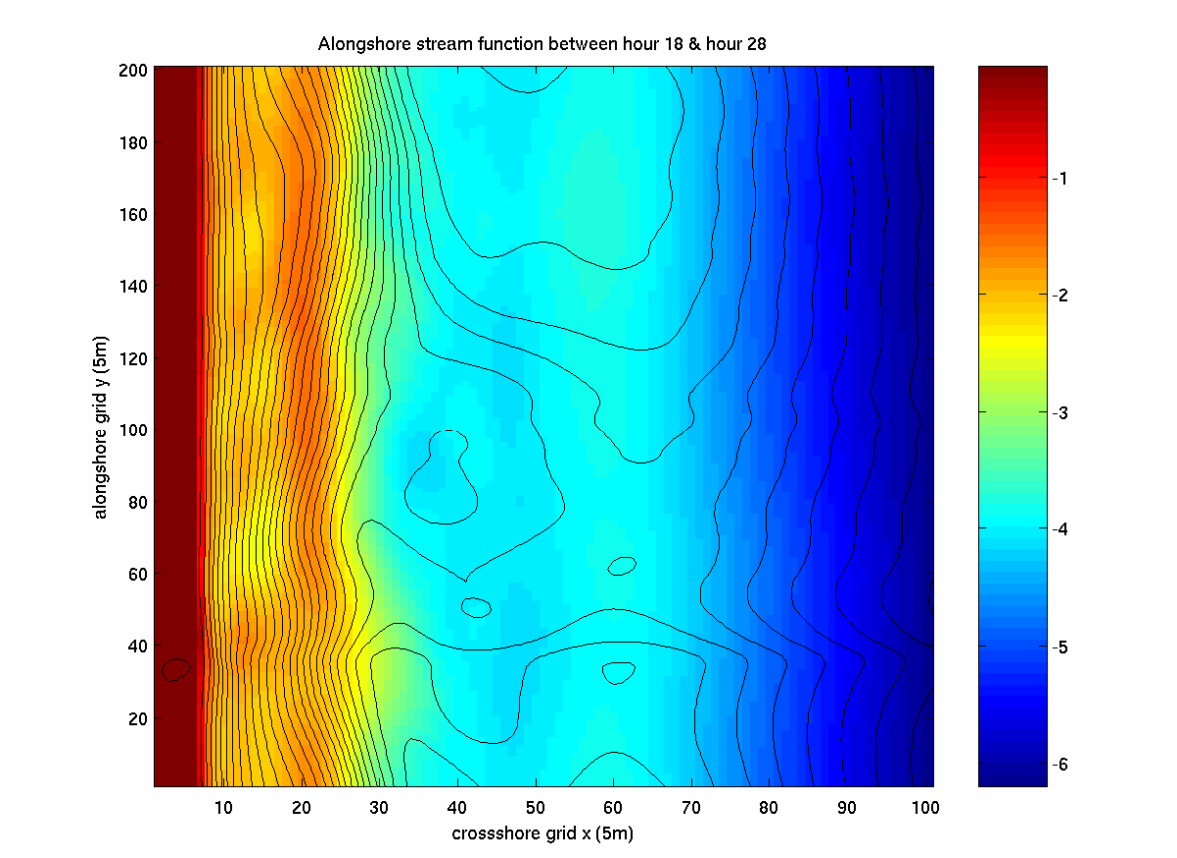

Figure 2-15. Time averaged alongshore stream function for November 6th.

A total net sediment transport for the simulation after 31 hours of wave action was completed but, due to the magnitude of the shoreline perturbations, it is difficult to analyze the sandbar region specifically. Here again, another simulation was run with the shoreline held static. This also allows the simulation to run for a full two days. In Figure 2-17 the sandbar region is looked at more closely. Wave height and wave direction stay consistent for the rest of the simulation; approximately one meter wave height and approach angle nearly shore normal. It is noted here again that holding the shoreline static did not significantly affect the magnitude or shape of the total net sediment transport.

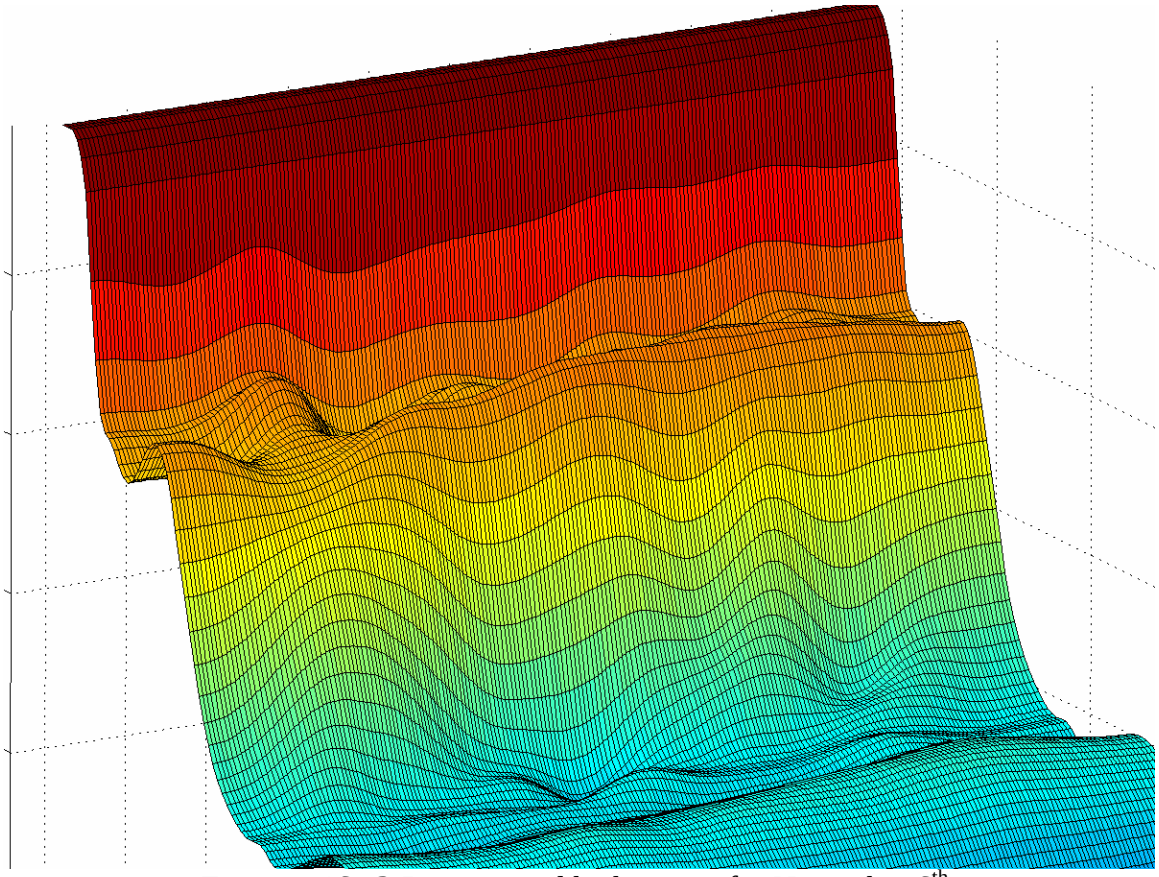

Figure 2-16. 3-Dimensional bathymetry for November 6th.

Similar to the NOV6 simulation, the magnitude of the sediment transport is also quite small; only about 35 cm of vertical change in the sandbar region. This is more likely to be an underestimate due to the fact that there is such an intense wave climate. The sediment transport in the sandbar region is nearly all moving onshore. The peak of the positive sediment transport is almost directly on top of the peak of the original sandbar and the depletion appears to be on the seaward slope of the bar. Again, the sediment transport seems to be building the bar more so than moving it. These magnitudes seem smaller than expected and the direction of transport seems suspect and will be discussed below, but the shape and areas of transport appear reasonable.

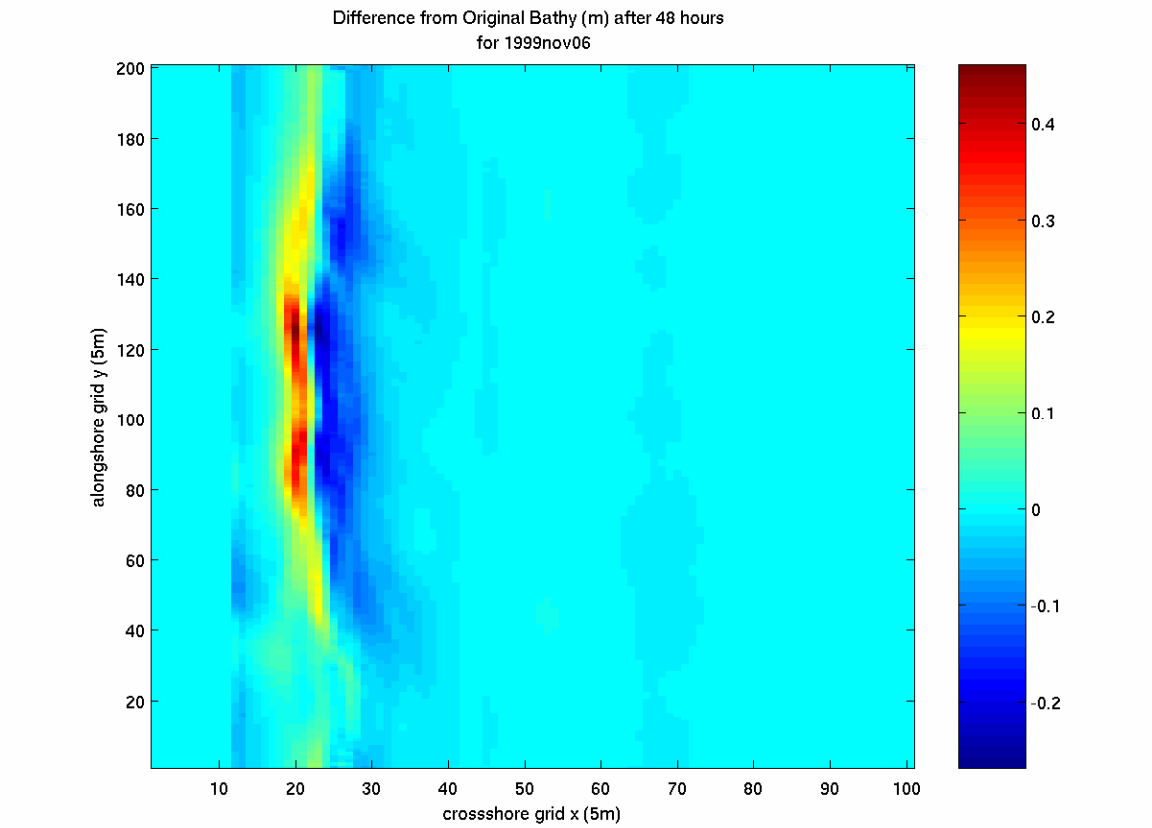

Figure 2-17. Difference in bathymetry for November 6th with the shoreline held static.

2.4.3 Comparison

OCT27's simulation as well as NOV6's simulation, to our judgment, produced less than expected sediment transport. The magnitude of transport is more acceptable for OCT27's case, because the wave climate is so mild, but seems more unrealistic for the case of NOV6's more energetic wave climate. It is hard to know what is sensible when comparable bathymetric surveys are spaced so far apart and the model is limited in time. The direction of transport correlates quite well with the stream line velocities of OCT27. With a straight and parallel initial sandbar, one would expect the shape of transport that was simulated for NOV6 but in the opposite direction. Sand bars on a natural beach typically move slowly shoreward when wave energy is low and move more rapidly offshore when waves are energetic and the wave driven circulation is strong [Winant et

al., 1975; Aubrey, 1979; Jaffe et al., 1984; Wright and Short, 1984; Lippmann and Holman, 1990]. With NOV6's vigorous wave climate, one would expect a net offshore sediment transport. As noted above, the net shoreward transport can be explained by the wave and current velocities co-aligning and reasonably dominating. Furthermore, for both simulations, the peaks of the sandbars don't seem to be moving very much but rather predominantly building and steepening the bar.

2.5 Discussion

Our model, which accounts for mean and oscillatory flow is based on the assumption that sediment suspension occurs instantaneously in response to fluid forcing. However, sediment suspension at one phase of the wave can be transported during a subsequent phase before settling to the bed [Hanes and Huntly, 1986]. Sediment transport where oscillatory flow is dominant, may also depend on fluid accelerations such as those caused by pressure gradients of the surface waves [Hallermeir, 1982; Hanes and Huntley, 1986; Gallagher, 1998] that are not accounted for in this model. With the fluid accelerations neglected, the alongshore current becomes an important mobilization force. Some have neglected this force [Bailard, 1981] but Thornton et al. [1996] found the best agreement between observed and predicted profile changes when the steady alongshore current contributed significantly to stirring of sediment that was subsequently transported offshore by the mean cross-shore flow.

Improved predictions of profile changes using the energetics transport model are reported to result from including (in the wave and wave-driven circulation models) undertow [Stive and Battjes, 1984], wave asymmetry [Nairn and Southgate, 1993], breaking-induced turbulence [Roelvink and Stive, 1989], and infragravity waves [Sato and Mitsunobu, 1991]. Recently published extensions of the Bailard [1981] model

[Hoefel and Elgar, 2003] demonstrated improved prediction skill compared to Gallagher, [1998], although the skill for the onshore bar migration sequence appears to be poorer than the results presented by Plant et al. [2004]. The extended models included a third-order statistic (i.e. skewness) of the acceleration computed from observed flow velocities. The timing of strong accelerations relative to onshore flow is hypothesized to produce net onshore sediment transport [Elgar et al., 2001]. Also added to their model were two additional free parameters, which will always increase the model hindcast skill [Davis, 1976].

A general inspection of parameterized nearshore process models by Plant et al. [2004] revealed that unresolved processes contribute to model errors. This suggests that additional information is necessary to adjust model parameters in order to minimize these errors. There is still not enough known about some of the processes that contribute to sediment transport. Dean and Dalrymple [2002] show the importance of the influence of wave-breaking-induced turbulence as a mobilizing agent within the surf zone. The dynamics of breaking waves on sand bars are understood only qualitatively. Gallagher [1998] suggests that vertical shear in mean cross-shore current may be significant. These various transport mechanisms are difficult to parameterize when little is known about them. To further complicate matters, their significance seems to vary with altering wave conditions. The relative importance of competing transport mechanisms is shown by Plant et al. [2001] to depend strongly on the relative wave height (defined as the ratio of the RMS wave height to the local depth).

The shape and direction of the sediment transport for the OCT27 simulation looks as expected, except for the fact that the oddities in the bar are not really smoothing out

but rather growing. This is an example of positive feedback. This is also the case for the shoreline perturbations which continue to grow and eventually make the model numerically unstable. In most cases in nature, there is negative feedback. When something gets out of equilibrium, nature usually slows it down and will try to bring it back. A good example of this is the air pressure of the earth. When there is a gradient of air pressure in the atmosphere, air in places of higher air pressure will shift air toward areas of lower pressure in the form of wind. Our model seems to have a positive feedback that must be addressed in future work. When a perturbation in the bathymetry is introduced, the model appears to magnify the disturbance rather than smooth it out as nature might under certain conditions. Not enough is known about all the mechanisms under shoaling waves to accurately predict or parameterize how this might be incorporated. Of course coastal zones also exhibit cases of positive feedback, in the form of erosional hotspots and non-uniform accretion to form beach cusps. Thus some of the model response, especially near the shoreline, may be representative of natural phenomenon.

An important thing to remember is that even an ideal sediment transport model can be inaccurate. First, performance of a sediment transport model is difficult to evaluate in studies where the predicted transport also depends on the accuracy of the hydrodynamic model, wave model, and underlying bathymetry. Secondly, errors in initial conditions, such as bathymetric sampling errors, could lead to errors in model predictions. For example, ripples that might significantly affect both hydrodynamics and sediment transport are not typically resolved by most surveying practices [Plant et al., 2002].

Accurate results may develop for flow over a smooth bed but may be inaccurate for flow over ripples and megaripples.

2.6 Conclusion

2.6.1 Future Work

The framework of a coupled beach morphology modeling system has been developed. It was tested for two data sets and environmental conditions at Duck, NC. The magnitude of sediment transport appears to be less than expected. Future work will include a more detailed study of the different components that contribute to sediment transport. From there, different coefficients can be assigned to various physically based terms accordingly to best fits to observations. Future work also includes modifications to attempt to numerically stabilize the shoreline region. When this is accomplished, model simulations should be able to run long enough in time to arrive at a second completed survey and model results can be compared to field data.

The direction of transport of the NOV6 simulation is a call for concern. The model predicted sediment transport onshore when offshore transport was expected. This can also be addressed in future work when additional mechanisms are added to the transport equation, such as undertow, skewness of waves, pressure gradient forces, and scour caused by breaking waves.

The hydrodynamics of the model are reasonable but include necessary engineering approximations for today's computational platforms. The alongshore stream function follows the bathymetry quite well with stronger flows developing in appropriate areas. The issues of shoreline retreat and advance and tidal variations in the water level eventually need to be addressed. The shoreline is an import boundary condition and

should be as representative as possible of natural conditions if accurate predictions are to be accomplished throughout the flow field.

2.6.2 Closing Remarks

The major achievement of this project has been to develop a rational framework for a beach morphology model coupled to a wave and mean current model and have it run continuously forced by measured data. With many of the correct physics represented in the model, the results are somewhat realistic but still considerably doubtful. This is considered acceptable because there is still much work to be done by the community to approximately represent more complex transport mechanisms. It is a vast problem and small steps are necessary.

There is still value in analyzing the results of the coupled modeling system we have implemented. First, because it is a step forward from where the community was. Second, because the formulas we used for sediment transport are widely accepted and used. And finally, because it allows a more simplified interpretation of the response of this still complex physical and modeling system. With reasonable results and the correct fundamental physics in place, it is quite encouraging and a good foundation for future development.

CHAPTER 3
PRESSURE GRADIENT FORCES AND SHEAR STRESSES ON SAND GRAINS UNDER SHOALING WAVES

3.1 Introduction

There is significant experimental evidence that flow acceleration, which serves as a proxy for the horizontal pressure gradient in a coastal bottom boundary layer, has an effect on sediment transport. This evidence originates from U-tube experiments [e.g., King, 1990], field measurements in the surf zone [e.g., Hanes and Huntley, 1986; Gallagher et al., 1998; Elgar et al., 2001] and in the swash [e.g., Butt and Russell, 1999; Puleo et al., 2003], and three-dimensional discrete particle computer simulations [e.g., Drake and Calantoni, 2001]. They have found significant correlations under certain relevant conditions between phases of flow acceleration caused by pressure gradient forces from the surface gravity waves and sediment suspension and net cross-shore transport. Hsu and Hanes [2004] demonstrate that responses of sheet flow, such as the velocity profiles, the instantaneous bed shear stress, the sediment flux, and the total amount of the mobilized sediment, cannot be fully parameterized by a quasi-steady free-stream velocity and may be correlated with the magnitude of the local horizontal pressure gradient. Moreover, their numerical experiments indicate that catastrophic internal bed failure is a direct consequence of large horizontal pressure gradients. These recent papers investigate the link between fluid acceleration and sediment transport. This chapter will explore the degree to which the pressure gradient contributes compared to the shear stress on sediment mobilization under surface gravity waves in the surf zone.

Generally there are two types of bed stresses that have the ability to mobilize sediment under surface gravity waves. One that is considered by all, is the shear stress exerted by the orbital velocities under a propagating wave. This stress results in a force acting tangentially to a surface such as a real flow over a sea bed. The other, maybe less recognized to have significance, is the horizontal pressure gradient stress. This stress is the consequence of the difference in hydrostatic pressure from one side of a particle to the other. When large enough, the difference in pressure can induce a sediment particle to become unstable and be mobilized.

In many typical coastal regimes, the ratio of the pressure gradient stress to the shear stress is 1/10 or even 1/50. For this reason, it has been thought sufficient to neglect the contribution of the pressure gradient stress in formulating the total stress in the surf zone. The primary aim of this study is to demonstrate that there is a regime in which it is inaccurate to neglect the pressure gradient stress. This will be done by examining such parameters as wave period, grain size, wave height, and water depth. A secondary aim is to obtain an understanding of the degree to which the pressure gradient stress contributes to bed mobilization to be used in future parameterizations of sediment transport models.

3.2 Stress Formulation

3.2.1 Shear Stress

The stress component from forces applied parallel to a surface is the shear stress. In our case, it is the force exerted by flowing water over a sea bed. We will be examining the shear stress resulting from this force. The stress is simply the force divided by the cross sectional area on which the force is applied. There is not a direct division of the cross sectional area in the shear stress, τ , equation because the grain size is embedded within the empirical Darcy-Weisbach friction factor *f*.

$$\tau = \tfrac{1}{8}\rho f u|u| \quad (3.1)$$

We are interested in the bottom shear stress, so the horizontal velocity term, *u*, is the horizontal near bottom fluid velocity. This variable will be examined more in section 3 below. The density of sea water is represented by ρ which has a value of $1024\,kg/m^3$.

This equation has been developed through dimensional analysis and experimental data have been used to develop values of the friction factor, *f*. For wave motion, the bottom friction is a nonlinear function and due to the absolute value sign becomes somewhat complicated to work with directly. In our model, the Stanton Diagram for friction factor under waves as a function of the relative roughness, *r*, was used to acquire the friction factor [Kamphuis, 1975]. Rough turbulent flow is assumed to obtain friction factors off of the Stanton diagram. A polynomial fit was then created to easily acquire friction factors for given parameters.

$$f = 0.62r^{-0.38} \quad (3.2)$$

It is important to note the ambiguity of the friction factor. The friction factors which are represented on the Stanton diagram are ones developed from measurements of bottom shear stress retarding the motion of a fluid in a unidirectional pipe flow. This leaves a bit of uncertainty in the level of approximation of this equation considering we are investigating sediment mobilization under surface gravity waves. We know that situations are seldom idealized. Therefore, possibly an empirical calculation, even if it is one derived from somewhat different circumstances, is a better representation of this physical occurrence. The evaluation of the shear stress equation is beyond the scope of this paper but the uncertainty and level of approximation inherent from representing it under ocean waves is not to be overlooked.

3.2.2 Pressure Gradient Stress

Under a surface gravity wave there is a variable water level within each wave. The difference in hydrostatic pressure from the differing water levels will exert a net horizontal force on a sand grain. Here we represent a sand grain as a sphere.

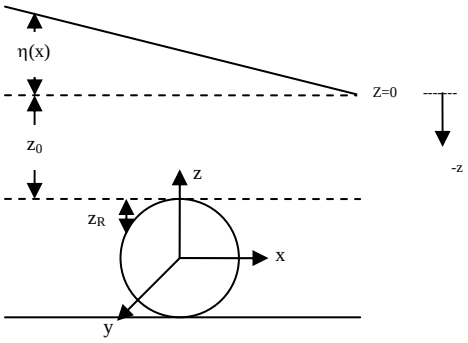

Figure 3-1. Schematic of a sand grain.

As everyone knows, sand grains are not perfect spheres, so a modest level of approximation is introduced at this point. The horizontal pressure gradient force is computed by integrating the normal force over the sphere surface. At each point on the surface of the sphere there is a force per unit area, *P*, on the solid acting normal to the surface. Multiplying this local force per unit area by the surface area on which it acts and integrating over the surface of the sphere will produce the resultant force.

$$F_x = \int_{\phi=0}^{\phi=2\pi} \int_{\theta=0}^{\theta=\pi} (-P\big|_{r=R} \sin\theta \sin\phi) R^2 \sin\theta d\theta d\phi \quad (3.3)$$

A detailed derivation of the resultant force can be found in the appendix. This force is analogous to a component of the inertial force calculation in the Morrison [1950] Equation.

$$F_I = \rho \forall (1 + C_m) \frac{du}{dx} \quad (3.4)$$

This equation is made up of two components

$$F_I = \rho \forall \frac{du}{dx} + C_m \rho \forall \frac{du}{dx} \quad (3.5).$$

The first part of this equation, or the "1" in equation 3.4, is the force that is corresponding to the pressure gradient force explained above.

This pressure gradient force is then divided by the cross sectional area on which the force is acting. The final stress can now be represented by

$$P_s = -\frac{4}{3} \rho g k_p \frac{\partial \eta}{\partial x} \frac{d_{50}}{2} \quad (3.6),$$

where the pressure stress is denoted as P_s, g is the acceleration due to gravity, $\partial \eta / \partial x$ is the local gradient of the wave in the horizontal direction, and k_p is the pressure response factor.

$$k_p = \frac{\cosh(k(h+z))}{\cosh(kh)} \quad (3.7)$$

An important point to note is that these two equations, whose magnitudes will be compared to each other, have a different designation for the grain size. The shear stress calculation uses d_{90} (diameter of the sand that 90% is finer) while the pressure stress calculation uses d_{50}. To account for this, the distribution of sand is assumed to obey a log normal probability distribution. That is, if normal probability paper is used for the cumulative percentage passing and the phi scale is used for the sand size, a straight line will result.

Again, there is always uncertainty with a completely idealized equation. There are no empirical parameters in this equation and we know that no situation is ever completely

idealized. Yet again, one must be cautious with the level of confidence put into an equation of this nature.

3.2.3 Phase Lag

The two stresses in question vary along time and space intervals as a surface gravity wave passes over a location. Hence, it is equivalent to examine a point in space over a wave period or different spatial locations at an instant in time. It was decided to hold the time variable constant and vary the space variable to investigate the distribution of the stresses. It was found that the peak stresses are separated by a phase lag of 90 degrees.

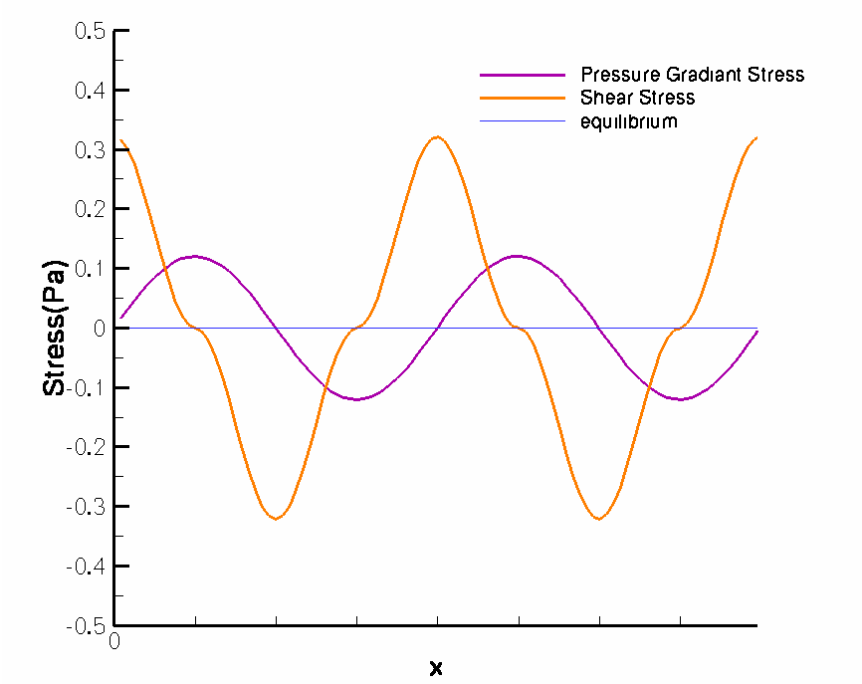

Figure 3-2. Phase lag of stresses.

Notice at some phases of the wave, the shear stress and pressure stress work together in a constructive manner and at other phases they work against each other in a destructive manner. Because the two phases lag by exactly 90 degrees, when one of the stresses is at its maximum, the other is zero.

It is not the individual stresses that will be compared to threshold values of mobilization but rather the total of the two which is the best indicator of bed mobilization. That is, the maximum of the total stress under the wave is the value that will be used to compare to the thresholds of mobilization to indicate whether a sand particle will be suspended under a wave for particular wave characteristics. A comparison of the two stress magnitudes at this certain phase, where the maximum total stress is found, will not be made but rather the maximum of each of the stresses under the wave will be compared. This is the only fair comparison because as alluded to before, there are parts under the wave which are completely dominated by the shear stress and others that are completely dominated by pressure stress. Comparing the two stresses at the point of maximum total stress is not as reasonable because the ratio would be swayed depending on where on the phase the total maximum stress was found. The reason to calculate the maximum total stress is to compare it to the threshold of mobilization to see if a particular sediment size will be suspended under certain conditions.

3.2.4 Nonlinear Wave

Everyone knows that ocean waves are not perfectly linear in nature. Many different types of nonlinearities exist. Especially as ocean waves approach breaking, a strong nonlinearity in the leading edge can be observed as a steep face. One can imagine that if a wave were to steepen, the steep leading edge of the wave would experience a far greater horizontal pressure gradient than the linear case.

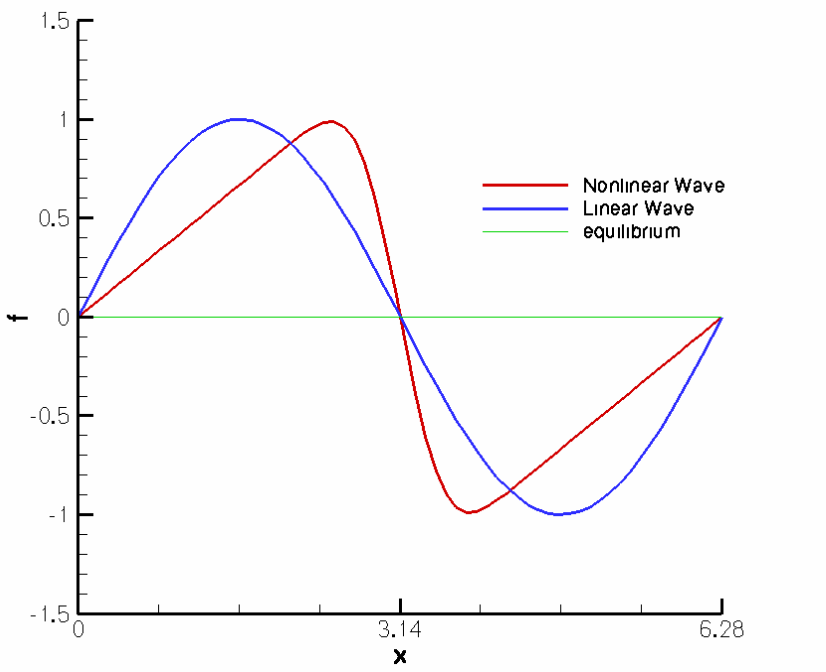

Figure 3-3. Nonlinear wave.

To analyze the contribution of the nonlinear wave it can first be broken down into many constituent waves by Fourier decomposition. A single nonlinear wave can be represented by a set of many smaller linear waves, all of them superimposed. Once broken down, the contribution by each smaller individual set of waves can be analyzed and tallied.

To find the phase position of the maximum total stress under a wave, only the first mode (1*x*) of the decomposition was varied. The nonlinear signal is not a complicated wave pattern, therefore most of the energy is found in the lowest frequency waves of the breakdown. Due to the fact that the nonlinear wave is of similar amplitude and frequency to the linear wave, the contributions of the multi-*x* waves drop dramatically after the 1*x* wave. In other words, only the lowest frequency of the stresses' decomposition is

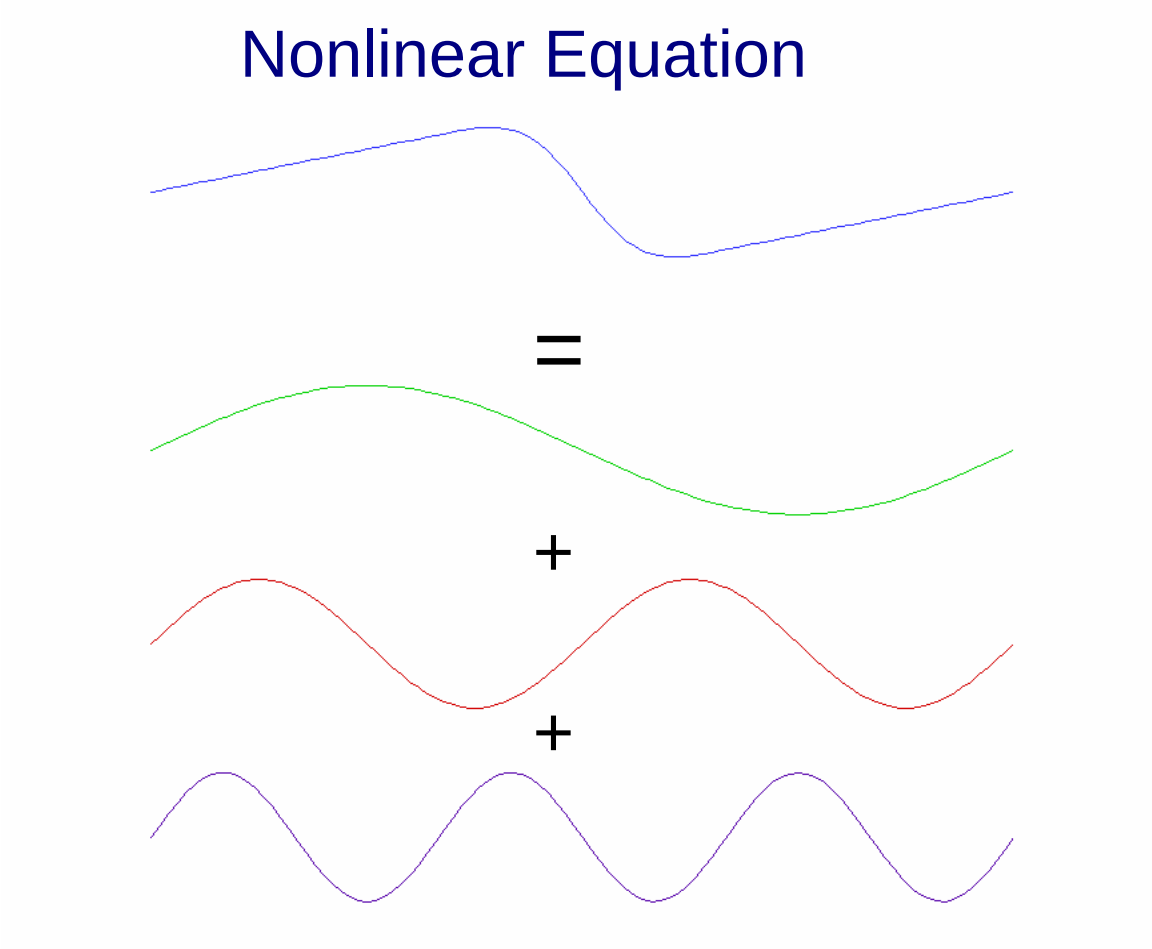

Figure 3-4. Nonlinear wave addition.

varied to find the maximum total stress phase position. The phase position is now used in the superposition of the remaining multi frequency waves.

Just as in the linear case, at some phases of the wave, one of the stresses will dominate the other stress. Although this time the maximum pressure gradient stress will be larger due to the steeper gradient and thus increase the ratio of pressure gradient stress to shear stress.

3.3 Varying Parameters and Limits

A closer look at the two stress equations reveals that they both decay exponentially with increasing *kh*. This *kh* parameter is the measure of wave type. Larger *kh* values indicate a more deep water wave ($kh > \pi$) and smaller *kh* values signify a more shallow

water wave ($kh < \pi/10$). Within the pressure gradient stress equation (eq. 3.4), the pressure response factor, k_p, includes the exponential function, hyperbolic cosine (or cosh).

$$\cosh(x) = \frac{e^{x} + e^{-x}}{2} \quad (3.8)$$

The exponential function is located in the denominator which will cause the magnitude of the pressure gradient stress to decay at a rate of e^{-kh}.

$$k_p = 1 \Big/ \cosh(kh) \quad \text{for the sea bed.} \quad (3.9)$$

Likewise, within the shear stress equation (eq. 3.1) the horizontal velocity, *u*, also includes the exponential function in the denominator.

$$u = gHk\cos(kx - \sigma t) \Big/ 2\sigma\cosh(kh) \quad \text{for the sea bed.} \quad (3.10)$$

The horizontal velocity is squared in the shear stress equation (eq. 3.1) while k_p is not raised to a power in the pressure gradient stress equation (eq. 3.4). Therefore, the magnitude of the shear stress will decay at a rate of e^{-2kh} while the pressure gradient stress will decay at a rate of e^{-kh}. At low values of *kh*, the shear stress is usually much more than the pressure gradient stress. With increasing *kh* values, both the stresses will decrease exponentially but the shear stress will decrease much faster. The magnitude of the pressure gradient stress will eventually overtake the magnitude of the shear stress. But will it be too much like a deep water wave when the pressure gradient stress has any sort of contribution? We are seeking to identify a realistic regime where the pressure gradient stress plays a substantial role in mobilizing sediment but is not in too deep of water that the combined stresses are too weak to initiate sediment movement.

This limits our analysis domain to inside the critical limit of mobilization. Our investigation is only shoreward of this point which is a function of grain size. These critical limits were first explored by Shields [1936]. He determined the threshold condition by measuring sediment transport for different values of total stress at least twice as large as the critical value and then extrapolated to the point of vanishing sediment transport. For turbulent flows over rough boundaries, the critical stress becomes linearly proportional to the sediment size. Based on a comparison of data from the Highway Research Board [1970], a relationship between critical stress and median grain size on a flat horizontal surface was formulated for granular material in table form [Julien, 1998]. A polynomial fit was then created to acquire a critical stress for a given sediment size.

$$\tau_{Critical} = 0.11 + 135.37 d_{50} + 225189.58 d_{50}^2 - 91766304.35 d_{50}^3 \quad (3.11),$$

where d_{50} is in meters and τ is measured in pascals.

The shoreward extent of our analysis domain will be taken at the breaker limit. Our analysis is based on linear theory which loses validity once a wave breaks. During breaking and after, other wave induced bed stresses become dominant like breaking-induced turbulence [Roelvink and Stive, 1989]. Therefore our analysis domain is limited to seaward of the break point. An approximate depth limited breaking boundary can be obtained from McCowan [1894], who determined that waves break when their height becomes equal to a fraction of the water depth.

$$H_b = 0.78 h_b \quad (3.12)$$

The subscript *b* denotes the value at breaking. This is a crude approximation and there has been more complex ways to acquire breaking parameters but this one will be used for simplicity.

Steepness limited breaking must also be taken into account. Miche [1944] developed a simple equation for wave breaking in any water depth.

$$\left(\frac{H}{L}\right)_{\max} = \frac{1}{7} \quad (3.13)$$

This indicates that the maximum wave height, *H*, is limited to one-seventh of the wave length, *L*. Also a crude approximation, but simply stated within our analysis.

3.4 Results

3.4.1 Linear Results

As stated above, shear stress dominates pressure stress in many typical wave conditions. An easy way to show this is by varying the water depth and seeing the resulting stresses for typical wave characteristics.

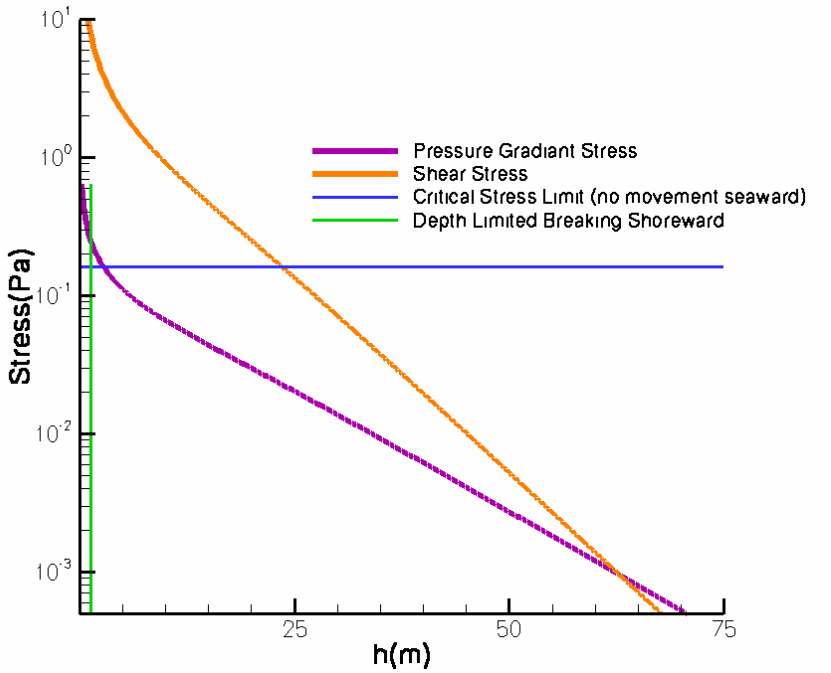

Figure 3-5. Linear: T = 7sec, d = 0.3mm, H = 1m

In Figure 3.5, the x-axis is the water depth measured in meters and the y-axis is the resulting stresses measured in pascals on a log scale. Here, the shear dominates well below the critical limit of mobilization.

The magnitude of the pressure force does eventually draw level and surpass the shear stress but this happens in water depths much too deep for the combination of the two stresses to initiate sediment mobilization.

This graph is a bit misleading because the intersections of either of the two stresses and the critical limit have no real significance. It is the addition of the two stresses which needs to be compared to the critical limit. It is not even the total of the two maximum stresses but rather the maximum of the total stress calculation under a wave which is being compared against the critical limit.

A better way to represent the stresses is to look at the ratio of the two stresses in question versus the *kh* parameter in which they vary so greatly.

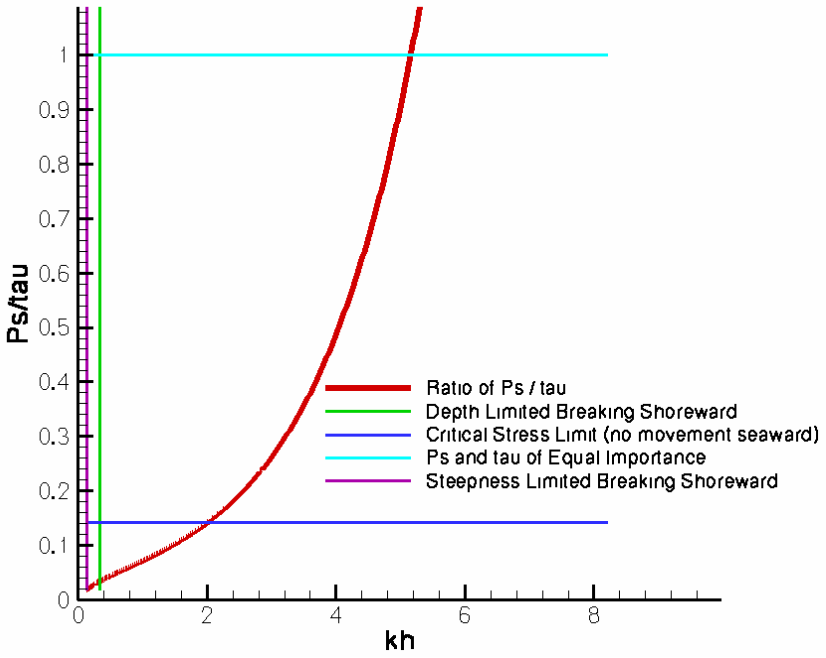

Figure 3-6. Linear: T = 7sec, d = 0.3mm, H = 1m

The x-axis is the non-dimensional wave type, *kh*, and the y-axis is the ratio of pressure gradient stress to shear stress. This way the graph is non-dimensional and the crossing of the ratio line and the critical limit has significance. This intersection will be the ratio of the maximum stresses just as an incoming wave initiates sediment motion. The greatest ratio will always occur at the offshore boundary when the critical stress is just met and the sediment is first mobilized. With these wave conditions the pressure gradient stress to shear stress ratio only reaches 0.14, or the magnitude of the pressure gradient stress is only 14% of that of the shear stress. With these wave conditions it seems reasonable to simply neglect the pressure gradient stress and still not sacrifice much accuracy.

Varying the dependant parameters, one can examine the relative importance of the pressure gradient stress to shear stress ratio. The wave height and period will remain the same and the diameter of the grains will be increased from 0.3 mm to 0.5 mm.

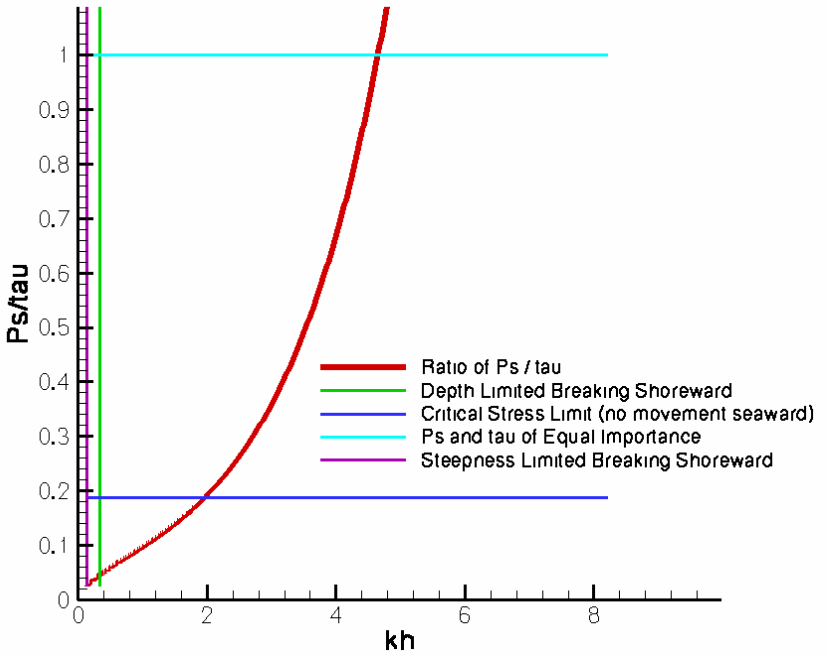

Figure 3-7. Linear: T = 7sec, d = 0.5mm, H = 1m

Here, the maximum ratio of pressure gradient stress to shear stress only increases slightly. The ratio only reaches a value around 0.18, still not very significant to the total stress contribution. An increase in the contribution of the pressure gradient stress implies that the greater surface area of a larger grain aids the pressure gradient stress more so than the shear stress, but only slightly.

The variation of the wave period will now be analyzed. The grain size diameter is returned to a value of 0.3 mm and the wave period is decreased from 7 seconds to 2.5 seconds. Decreasing the wave period and keeping the same wave height will effectively make the wave shorter and steeper. This will cause a bigger disparity of hydrostatic pressure from one side of a sand grain to the other.

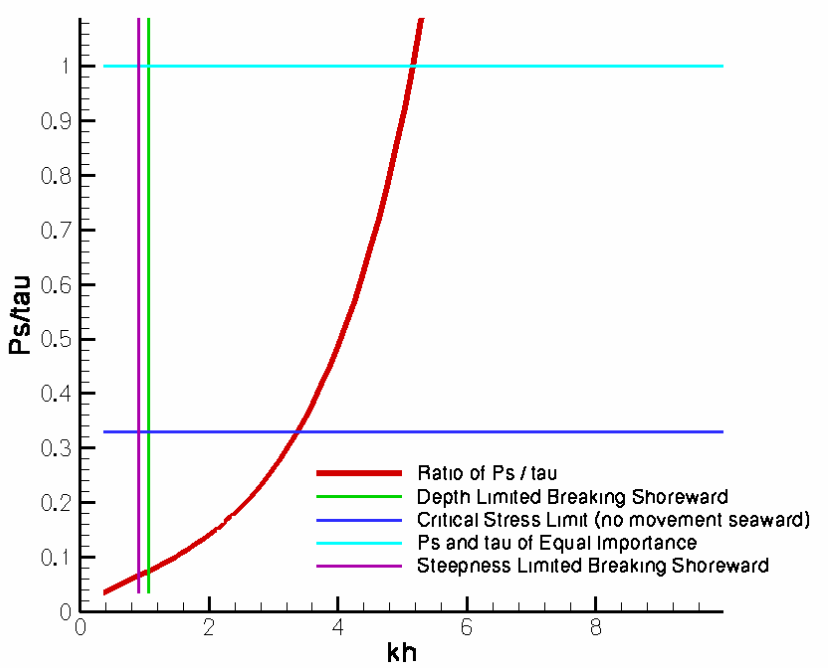

Figure 3-8. Linear: = 2.5sec, d = 0.3mm, H = 1m

In this example, the ratio of pressure gradient stress to shear stress has increased noticeably by making the wave period shorter. The ratio at the point of mobilization has increased to over 0.3. With such a short wave, one must be conscious of the wave being

too steep and breaking. Here, the graph also indicates that the wave will break due to depth limited breaking before it reaches its steepness limitation.

The wave height was also varied, but little change in maximum ratio was observed. The only noticeable outcome was a change in the break point. The increased wave height may mobilize a greater domain of sediment but our domain of applicability decreased because the breaker limitation and the maximum ratio remain similar.

With the wave period shortened and the grain size increased, the pressure stress will find its most favorable contribution. In the next case, the wave period is shortened again to 2.5 seconds and the grain size diameter is increased to 0.5 mm. With these wave characteristics, the maximum pressure stress to shear stress ratio has now reached 0.42.

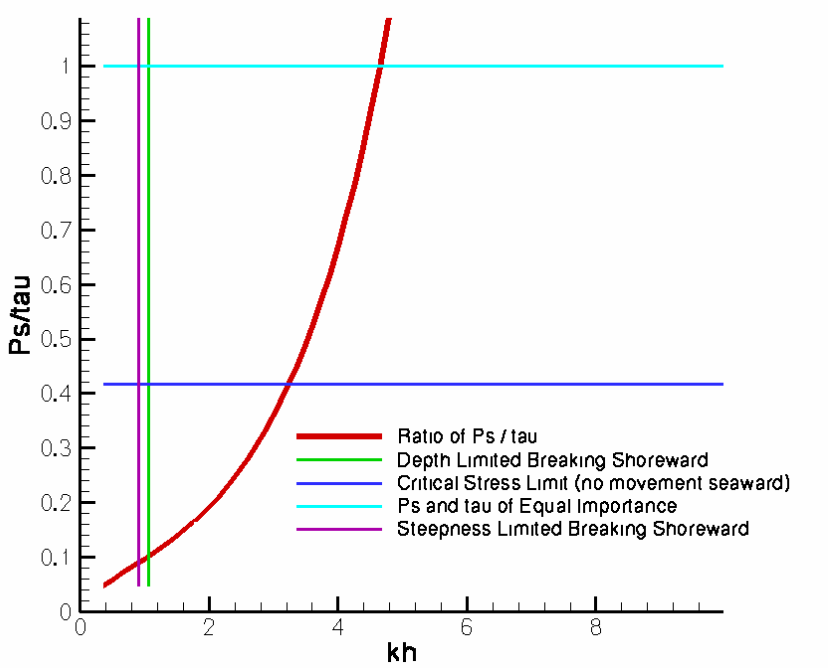

Figure 3-9. Linear: T = 2.5sec, d = 0.5mm, H = 1m

Note where the sediment is mobilized along the kh axis. At the point of mobilization the kh value is 3.2 and at the point of breaking the kh value is 1.5. Here our analysis domain falls within the intermediate wave type category.

3.4.2 Nonlinear Results

The nonlinear results will be analyzed in a similar fashion to the linear case. Similar results are observed but swayed more toward the contributions from the pressure gradient. Figure 3-10 shows the dimensional graph varying the water depth and viewing the resulting stresses.

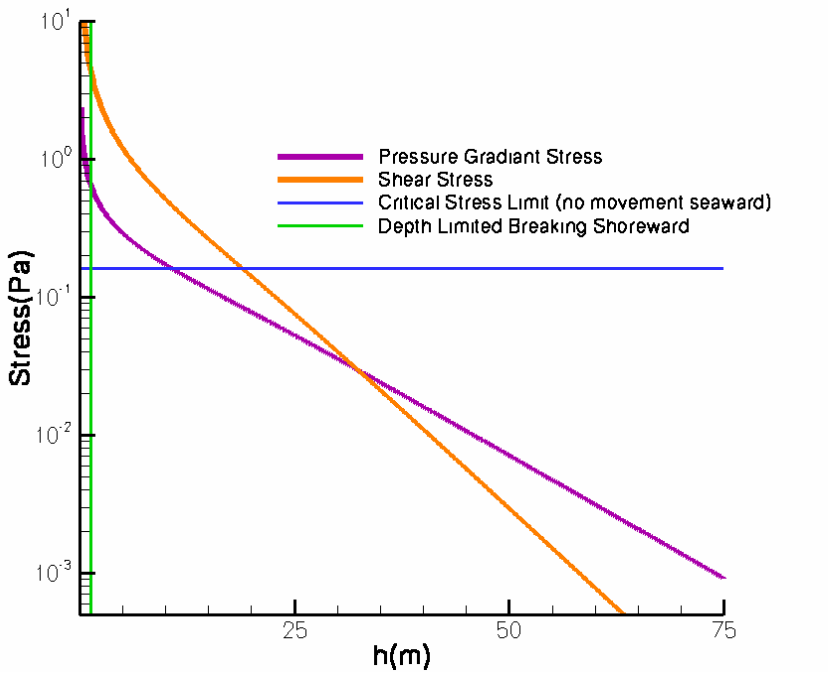

Figure 3-10. Nonlinear: = 7sec, d = 0.3mm, H = 1m

This again is for our proto-typical wave conditions. With the same axis lengths and scale as the linear graph, it is apparent that the shear stress and pressure gradient stress crossing point occurs in much shallower water and closer to the critical limit. What also should be understood from this graph is that there is a regime from about 10 meters water depth into the break limit where the pressure stress alone is enough to mobilize the sediment.

The nonlinear case is also converted to a non-dimensional graph in Figure 3-11. The stresses are represented as the ratio of maximum pressure to shear stress and the *kh* parameter is varied.

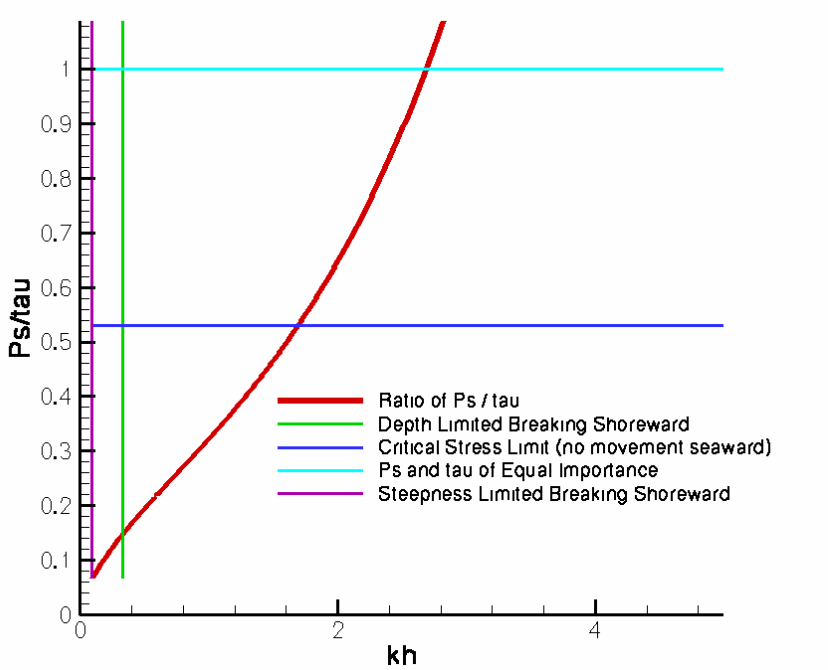

Figure 3-11. Nonlinear: T = 7sec, d = 0.3mm, H = 1m

The ratio at the point of mobilization has increased to over 0.5. This is considerably larger compared to the linear case, 0.14, with the same wave characteristics.

The same dependant variables will be varied with the nonlinear wave at the same degree to see its effect on the stresses compared to that of the linear case. First the grain size diameter will be increased to 0.5 mm. The increase in grain size diameter has a similar effect as the linear case. The change in grain size results in a minimal change of the maximum ratio. The pressure gradient stress to shear stress ratio has now reached a value of 0.7. Figure 3-12 shows that the maximum of the pressure gradient stress and the shear stress are now nearly the same magnitude at the point of mobilization.

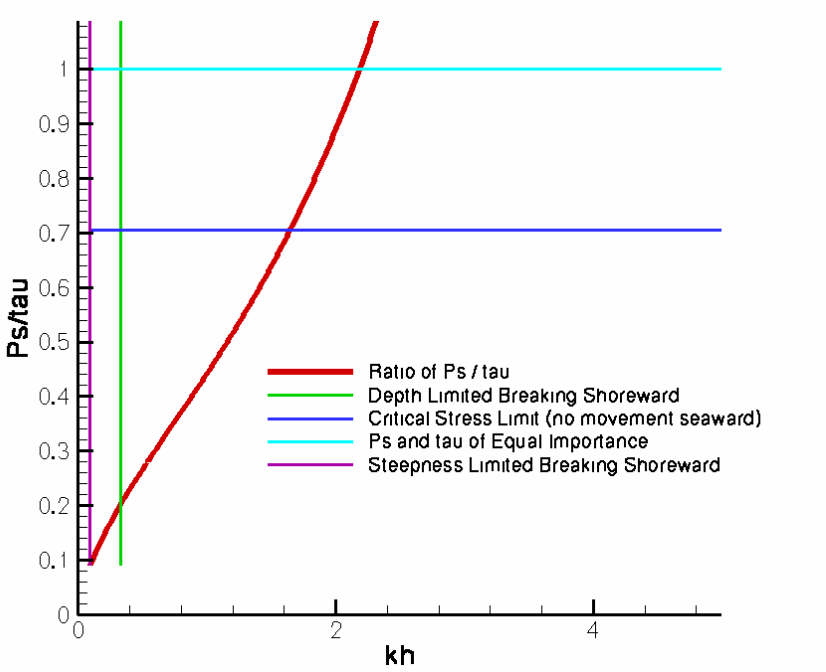

Figure 3-12. Nonlinear: T = 7sec, d = 0.5mm, H = 1m

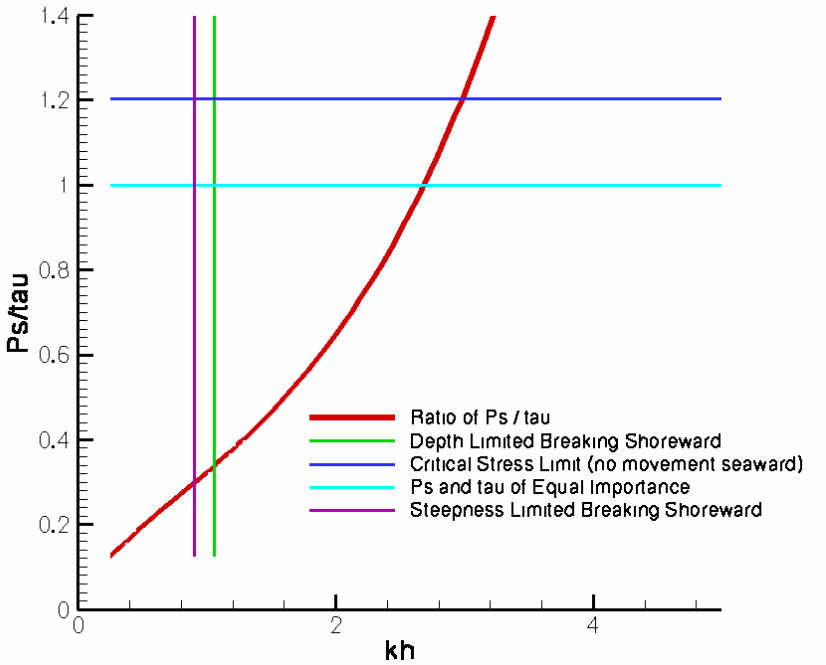

Figure 3-13. Nonlinear: T = 2.5sec, d = 0.3mm, H = 1m

The grain size is returned to 0.3 mm and the wave period is now decreased to 2.5 seconds in figure 3-13. With the ratio of the stresses reaching and surpassing 1.0 and the sediment still being mobilized, the magnitude of the pressure gradient stress is now more

than the shear stress just as the sediment is mobilized. At the point of mobilization the pressure gradient stress is about 20% greater than the shear stress.

The wave height has little effect as mentioned earlier in the linear case. The two dependent variables, wave period and grain size, make the largest contributions to maximizing the contribution of the pressure gradient stress.

Similar to the linear case, the grain size and wave period are changed to maximize the contribution by the pressure gradient stress.

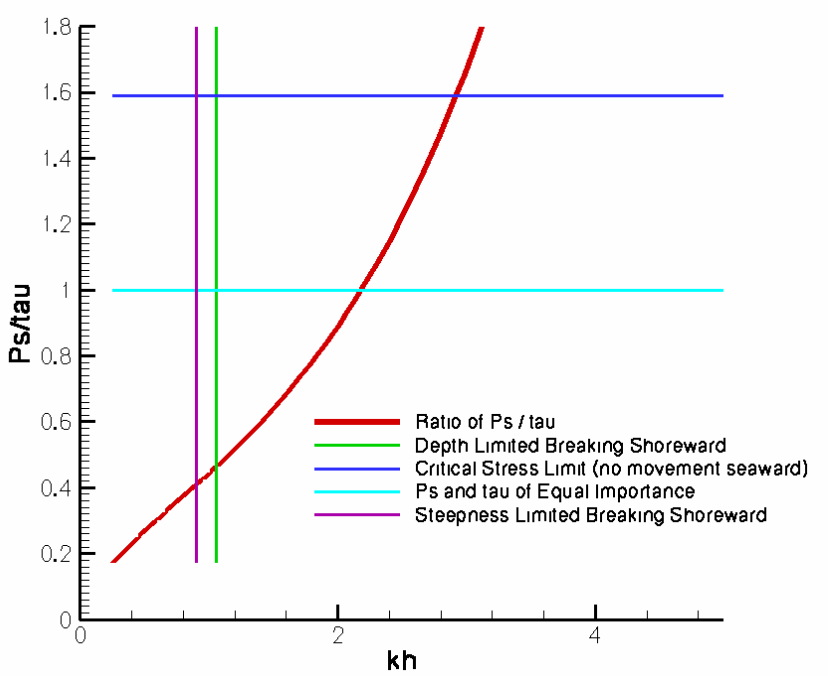

Figure 3-14. Nonlinear: T = 2.5sec, d = 0.5mm, H = 1m

The ratio has now reached 1.6 at the point of mobilization. The magnitude of the maximum pressure gradient stress is 60% greater than that of the shear stress at the point of mobilization. The *kh* axis indicates again that our analysis takes place within the intermediate wave type range.

3.5 Conclusion

A simple analytical model based on empirical formulas was used to examine the relative contributions of pressure and shear stresses to bed mobilization. First, the parameters that were varied will be discussed. It became evident that an increase in grain size diameter contributed to the pressure gradient stress contribution. Clearly a larger surface area for the horizontal pressure gradient force to act upon is more favorable then for the shear force to act upon. A decrease in wave period also produced a favorable contribution for the pressure gradient stress. A decreased period will result in a shorter and steeper wave. The steeper gradient will result in a greater horizontal pressure gradient and a noticeably greater pressure gradient stress contribution. Both changes in these parameters are in favor of the pressure gradient stress but to different degrees. The dependent variable comparison gives the impression that the ratio of the two stresses is more sensitive to the change in wave period rather than grain size. As mentioned before, the wave height appeared to have minimal effect on the ratio. While the break point would move, the maximum ratio of pressure gradient stress to shear stress stayed approximately the same.

The analysis gives us some distinct regimes where the pressure gradient stress holds considerable influence on the total stress. Short period waves, 2 - 5 seconds, will result in an influential contribution by the pressure gradient stress. For a 2.5 second wave and 0.3 mm grain size, the magnitude of the maximum pressure gradient stress reaches over 30% of that of the shear stress for the linear wave case and is actually 20% more than the maximum shear stress for the nonlinear wave case. The solutions also show that it was not uncommon for the pressure gradient stress alone to be sufficient to induce particle mobilization. This suggests that for short period waves, the pressure gradient

stress can be quite important. Increased grain size also resulted in an enhanced contribution by the pressure gradient stress, but not to the extent of the wave period fluctuations. Larger grain sizes, 0.3- 1.0 mm, appear to favor the pressure gradient contribution. These characteristics were developed for our analysis in intermediated water depths, 1-15 meters, and resulted in intermediate wave types.

Altering both the wave period and the grain size to realistic ocean quantities, a 2.5 second wave and a mean sand grain diameter of 0.5 mm, one can detect a significant contribution from the pressure gradient stress. The linear case suggests that the magnitude of the maximum pressure gradient stress is over 40% to that of the maximum shear stress while the nonlinear case indicates that the pressure gradient stress is actually 60% more than that of the shear stress when the sediment is first mobilized. One certainly can not have much confidence in setting a threshold for the total stress when possibly half the magnitude of the stress is neglected if pressure gradient contributions are neglected.

The analysis has also shown where the pressure gradient stress makes its greatest contribution. The maximum contribution made by the pressure gradient stress was always located at the critical point of mobilization or more easily stated, just as an incoming wave begins to move sediment around. This is also the place within our analysis domain where a wave exhibits its most linear form. As a wave approaches breaking, it will take on more of a nonlinear form similar to the one analyzed in this study. A breaking wave may even approach a vertical wall of water just prior to breaking which would increase the pressure gradient stress significantly. This suggests that the pressure gradient stress could become important along our entire analysis domain, from

the critical stress limit all the way to the point of breaking. Consequently, for certain wave and grain characteristics, it would be precarious to not include the pressure gradient stress in the total stress calculation and expect high levels of precision.

Since the pressure gradient stress caused by surface gravity waves show some relative contribution to the total stress at the sea-bed, one must rethink the way that near shore sediment transport parameterizations are found. These parameterizations should not be reasonably based upon empirical relationships developed from open channel or even oscillatory flow experiments if they are not produced by surface gravity waves. By including pressure gradient stresses it will also help in the parameterization of sediment flux in the direction of wave advance due to asymmetric and skewed nonlinear wave shapes typical of shoaled and breaking waves.

APPENDIX
DERIVATION OF THE RESULTANT FORCE ON A SPHERE

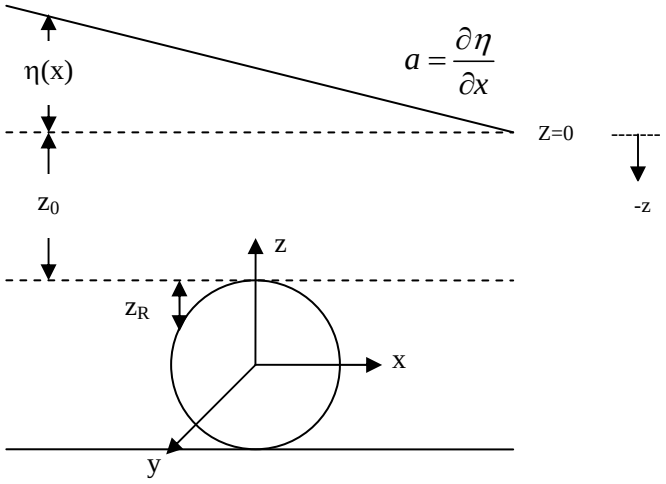

$$\eta(x) = ax$$
$$z_R = R\cos\theta$$

$$F_x = \int_{\phi=0}^{\phi=2\pi}\int_{\theta=0}^{\theta=\pi}(-P\big|_{r=R}\sin\theta\sin\phi)R^2\sin\theta d\theta d\phi$$

$$P\big|_{r=R} = P_{atm} + \rho g z_0 + \rho g\,\eta(x)\big|_{r=R} + \rho g z_R$$
$$P\big|_{r=R} = P_{atm} + \rho g z_0 + \rho g a R\sin\theta\sin\phi + \rho g R\cos\theta$$

$$F_x = \int_0^{2\pi}\int_0^{\pi}\{-[P_{atm} + \rho g z_0 + \rho g a R\sin\theta\sin\phi + \rho g R\cos\theta]\sin\theta\sin\phi\}R^2\sin\theta d\theta d\phi$$
$$F_x = \int_0^{2\pi}\int_0^{\pi} -P_{atm}R^2\sin^2\theta\sin\phi d\theta d\phi + \int_0^{2\pi}\int_0^{\pi} -\rho g z_0 R^2\sin^2\theta\sin\phi d\theta d\phi$$
$$+\int_0^{2\pi}\int_0^{\pi} -\rho g a R^3\sin^3\theta\sin^2\phi d\theta d\phi + \int_0^{2\pi}\int_0^{\pi} -\rho g R^3\cos\theta\sin^2\theta\sin\phi d\theta d\phi$$

$$F_x = \int_0^{\pi} -\rho g a R^3 \sin^3\theta \cdot \left(\frac{\phi}{2} - \frac{\sin 2\phi}{4}\right)\Bigg|_{\phi=0}^{\phi=2\pi} d\theta = \int_0^{\pi} -\pi\rho g a R^3 \sin^3\theta \, d\theta$$

$$F_x = \int_0^{\pi} -\pi\rho g a R^3 \cdot -\frac{1}{3}\cos\theta(\sin^2\theta + 2)\Bigg|_{\theta=0}^{\theta=\pi} \qquad F_x = -\frac{4}{3}\pi\rho g a R^3$$

$$\frac{F_x}{A_p} = \frac{-\frac{4}{3}\pi\rho g a R^3}{\pi R^2} = -\frac{4}{3}\rho g a R = P_s = -\frac{4}{3}\rho g k_p \frac{\partial\eta}{\partial x}\frac{d_{50}}{2}$$

LIST OF REFERENCES

Aubrey, D.G., Seasonal patterns of onshore/offshore sediment movement, *J. Geophys. Res., 84,* 6347-6354, 1979.

Bagnold, R.A., Mechanics of marine sedimentation, in *The Sea*, vol. 3, *The Earth Beneath the Sea*, edited by M.N. Hill, pp 507-528, Wiley-Interscience, New York, 1963.

Bagnold, R.A., An approach to the sediment transport problem from general physics, *Prof. Paper 422-I* U.S. Geol. Surv., 1966.

Bailard, J.A., An energetics total load sediment transport model for a plane sloping beach, *J. Geophys. Res., 86,* 10938-10954, 1981.

Bailard, J.A., and D.L. Inman, An energetics bedload transport model for a plane sloping beach: local transport, *J. Geophys. Res., 86,* 2035-2043, 1981.

Birkemeier, W.A. and C. Mason, The crab: A unique nearshore surveying vehicle, *J. Surv. Eng., 110,* 1-7, 1984.

Birkemeier, W.A. and K.T. Holland, The corps of engineers' field research facility: More than two decades of coastal research. *Shore Beach, 69,* 3-12, 2001.

Booij, N., R.C. Ris, and L.H. Holthuijsen, A third generation wave model for coastal region: 1. Model description and validation, *J. Geophys. Res., 104,* C4, 7649-7666, 1999.

Bowen, A.J., Simple models of nearshore sedimentation; beach profiles and longshore bars, in *The Coastline of Canada*, edited by S.B. McCann, Geol. Surv. Of Can. *Papp. 80-10*, pp 1-11, Ottawa, 1980.

Butt, T. and P. Russell, Suspended sediment transport mechanism in high-energy swash, *Mar. Geol. 161,* 361-375, 1999.

Conley, D.C. and D.L. Inman, Ventilated oscillatory boundary layers, *J. Fluid Mech., 273,* 261-284, 1994.

Davis, R.E., Predictability of sea surface temperature and sea level pressure anomalies over the North Pacific Ocean, *J. Phys. Oceanogr., 6,* 249-266, 1976.

Dean, R.G. and R.A. Dalrymple, *Coastal Processes with Engineering Applications*, Cambridge University Press, Cambridge, 2002.

Downing, J.P., R.W. Sternberg, and C.R.B. Lister, New instrumentation for the investigation of sediment suspension processes in the shallow marine environment, *Mar. Geol., 42*. 19-34, 1981.

Drake, T. G. and J. Calantoni, Discrete particle model for sheet flow sediment transport in the nearshore, *J. Geophys. Res., 106*(C9), 19,859-19,868, 2001.

Elgar, S., E.L. Gallagher, and R.T. Guza, Nearshore sandbar migration, *J. Geophys. Res., 106*, C6, 11623-11627, 2001.

Fedderson, F., R.T. Guza, S., and T.H.C. Herbers, Velocity moments in alongshore bottom stress parameterizations, *J. Geophys. Res., 105*, 8673-8686, 2000.

Foster, D.L., R.A. Holman, and R.A. Beach, Sediment suspension events and shear instabilities in the bottom boundary layer, in *Coastal Dynamics '95*, pp 712-726, Am. Soc. Of Civ. Eng., New York, 1995.

Gallagher, E.L., Observations of sand bar evolution on a natural beach, *J. Geophys. Res., 103*, 3203-3215, 1998.

Hanes, D.M. and D.A. Huntley, Continuous measurements of suspended sand concentration in a wave dominated nearshore environment, *Cont. Shelf Res., 6*, 585-596, 1986.

Hay, A.E. and A.J. Bowen, Coherence scales of wave-induced suspended sand concentration fluctuations, *J. Geophys. Res., 99*, 12, 749-12,765, 1994.

Heath, M.T., *Scientific Computing: An Introductory Survey*, Second Edition, pp 407-410, McGraw-Hill, New York, 2002.

Highway Research Board, Tentative design procedure for riprap-lined channels, *National Academy of Science, National Cooperative Highway Research Program*, Report no. 108, 1970.

Hoefel, F. and S. Elgar, Wave-induced sediment transport and sandbar migration, *Science*, 299, 1885-1887, 2003.

Holland, K.T., C.L. Vincent, and R.A. Holman, Statistical characterization of nearshore morphodynamic behavior, in *Coastal Sediments '99*, edited by N.C. Kraus, pp 2176-2189, Am. Soc. Of Civ. Eng., Reston, Virginia, 2000.

Hornbeck, R.W., *Numerical Methods*, Prentice-Hall, New Jersey, 1975.

Hsu, T.-J. and D.M. Hanes, Effects of wave shape on sheet flow sediment transport, *J. Geophys. Res.*, 109, C05025, doi:10.1029/2003JC002075, 2004.

Jaffe, B.E., R.W. Sternburg, and A.H. Sallenger, The role of suspended sediment in shore-normal beach profile changes, in *Proc. 19th Int. Coastal Eng. Conf*., pp 1983-1996, Am. Soc. of Civ. Eng., New York, 1984.

Julien, P.Y., *Erosion and Sedimentation*, Cambridge University Press, New York, 1998.

Kamphuis, J.W., Friction factor under oscillatory waves, *J. Waterways, Harbors Coastal Eng. Div., ASCE*, Vol. 101, 135-144, 1975.

King, D.B., Studies in oscillatory flow bed load sediment transport, Ph.D. thesis, University of California, San Diego, 1990.

Lippmann, T.C. and R.A. Holman, The spatial and temporal variability of sand bar morphology, *J. Geophys. Res., 95*, 11575-11590, 1990.

Longuet-Higgins, M.S. and R.W. Stewart, The changes in the form of short gravity waves on steady non-uniform currents, *J. Geophys. Res., 8*, 565-583, 1960.

Longuet-Higgins, M.S. and R.W. Stewart, Radiation stress in water waves, a physical discussion with application, *Deep Sea Res., 11*, 529-563, 1964.

McCowan, J., On the Highest Wave of Permanent Type, *Philos. Mag. J. Sci.*, Vol. 38, 1894.

McIlwain, S. and D.N. Slinn, Modeling alongshore currents over barred beaches, submitted to the *Journal of Waterway, Port, Coastal, and Ocean Engineering*, 2004.

Miche, M., Movements ondulatoires des mers en profondeur constante ou decroissante, *Annales des Ponts et Chaussees*, 25-78, 131-164, 270-292, 369-406, 1944.

Morrison, J.R., M.P. O'Brien, J.W. Johnson, and S.A. Schaaf, The force exerted by surface waves on piles, *Petrol. Trans., AIME*, Vol. 189, 1950.

Nairn, R.B. and H.N. Southgate, Deterministic profile modeling of nearshore processes. Part 2. Sediment transport and beach profile development, *Coastal Eng., 19*, 57-96, 1993.

Ozkan-Haller, H.T. and J.T Kirby, Nonlinear evolution of shear instabilities of the longshore current: A comparison of observations and computations, *J. Geophys. Res., 104*, C11, 25953-25984, 1999.

Plant, N.G., R.A. Holman, M.H. Freilich, and W.A. Birkemeier, A simple model for interannual sandbar behavior, *J. Geophys. Res., 104*, 15, 755-15, 776, 1999.

Plant, N.G., B.G. Ruessink, and K.M. Wijnberg, Morphologic properties derived from a simple cross-shore sediment transport model, *J. Geophys. Res., 106*, 945-958, 2001.

Plant, N.G., K.T. Holland, and J.A. Puleo, Analysis of the scale of errors in nearshore bathymetric data, *Mar. Geol., 191*, 71-86, 2002.

Plant, N.G., K.T. Holland, J.A. Puleo, and E.L. Gallagher, Prediction skill of nearshore profile evolution models, *J. Geophys. Res., 109*, C01006, 2004.

Puleo, J.A., K.T. Holland, N.G. Plant, D.N. Slinn, and D.M. Hanes, Fluid acceleration effects on suspended transport in the swash zone, *J. Geophys. Res., 108*(C11), 3350, doi:10.1029/2003JC001943, 2003.

Roelvink, J.A., and M.J.F. Stive. Bar generating cross shore flow mechanisms on a beach, *J. Geophys. Res., 94*, 4785-4800, 1989.

Roelvink, J.A. and I. Broker, Cross-shore profile models, *Coastal Eng., 21*, 163-191, 1993.

Sato, S. and N. Mitsunobu, A numerical model of beach profile change due to random waves, in *Proc. Coastal Sediments '91*, pp 674-687, Am. Soc. of Civ. Eng., New York, 1991.

Shields, A., Anwendung der aehnlichkeitsmechanik und der turbulenz forschung auf die geschiebebewegung, *Mitteilungen der Preussische Versuchanstalt fur Wasserbau und Schiffbau*, Berlin, 1936.

Sleath, J.F.A., *Sea Bed Mechanics*, pp 335, John Wiley, New York, 1984.

Slinn, D.N., J.S. Allen, P.A. Newberger, and R.A. Holman, Nonlinear shear instabilities of alongshore currents over barred beaches, *J. Geophys. Res., 103*, 18, 357-18, 379, 1998.

Slinn, D.N., J.S. Allen, and R.A. Holman, Alongshore currents over variable beach topography, *J. Geophys. Res., 105*, C7, 16,971-16,998, 2000.

Stauble, D.K., Long-term profile and sediment morphodynamics: Field Research Facility case history, *Tech. Rep. CERC-92-7*, U.S. Army Corp of Eng., 1992.

Stive M.J.F., A model for cross-shore sediment transport, in *Proc. 20th Int. Coastal Eng. Conf.*, pp 1550-1564, Am. Soc. of Civ. Eng., Taipei, Taiwan, 1986.

Stive M.J.F. and J.A. Battjes, A model for offshore sediment transport, in *Proc. 19th Int. Coastal Eng. Conf.*, pp 1420-1436, Am. Soc. of Civ. Eng., New York, 1984.

Svendsen, I.A. and U. Putrevu, Nearshore mixing and dispersion, *Proc. R. Soc. London, Ser. A, 445*, 561-576, 1994.

Thornton, E.B., R.T. Humiston, and W.A. Birkemeier, Bar-trough generation on a natural beach, *J. Geophys. Res., 101*, 12097-12110, 1996.

Winant, C.D., D.L. Inman, and C.E. Nordstrom, Description of seasonal beach changes using empirical eigenfunctions, *J. Geophys. Res.*, *80*, 1979-1986, 1975.

Wright, L.D. and A.D. Short, Morphodynamic variability of surf zones and beaches: a synthesis, *Mar. Geol.*, *26*, 93-118, 1984.

BIOGRAPHICAL SKETCH

I was born and in a small coastal town located on the New Jersey Shore called Point Pleasant. I spent my first 6 years in a small house in Toms River, NJ, only to move to a more rural area located just south. It is here in Lanoka Harbor that I spent the majority of my adolescence. In this house I lived with my two loving parents and my older sister, Maggie. I was also blessed with the great experience of living with my grandparents too.

Growing up in this small pristine town was very enjoyable. I spent the majority of my time outside playing sports, surfing, and riding my bike with my friends. As I grew older, I became more involved in organized sports. By high school I participated in three varsity sports (football, indoor track, and baseball) and was the captain of two by senior year. I was also very active in many clubs and groups as well as playing in the marching band for one year.

After graduating high school in 1999 I decided to attend North Carolina State University. It was not an easy decision, because going to a large university meant that it would be difficult to play any varsity sport. I got involved in different ways by joining a social fraternity (Sigma Chi) as well as an honors fraternity (Chi Epsilon). Being the intramural sports chairman and participating in philanthropy events around the community were a few ways I spent my free time in college. I was even able to play a varsity sport when I walked onto the track team for one year.

Of course the academic demands of civil engineering were first and foremost. I feel I was provided with an excellent base of skills in civil engineering at NC State to excel in any sub discipline chosen. It was my junior year, after I heard a presentation by one of our professors, that I knew coastal engineering was the field for me. It combined something I enjoyed studying, engineering, as well as something I loved, the beach. I was fortunate enough to obtain an internship in Duck, NC at the USACE Field Research Facility for the summer after my junior and senior years of undergraduate. Here I got a taste of the coastal engineering field by participating in many field experiments and leading a public tour.

After graduating from NC State University in May of 2003, it seemed like an easy decision to continue my academic experience in graduate school studying coastal engineering at the University of Florida. The decision was made easier after being offered a graduate research assistant position studying under Dr. Donald Slinn. I have demonstrated growth and development in my short time at U.F. by speaking and presenting at two major conferences and expect to have two papers published from my thesis work. While working under Dr. Slinn I also managed to have a successful internship at the Naval Research Laboratory and will be graduating with honors this summer with my Master of Science degree.

This August I begin my practical coastal engineering experience when I start a full time job with Olsen & Associates, a small coastal engineering firm located in Jacksonville, FL. I am eager to apply my knowledge in a practical atmosphere and am also excited about my short move to the Jacksonville area.